J. metamorphic Geol., 1994, **12**, 49–68

Jadeitites, albitites and related rocks from the Motagua Fault Zone, Guatemala

G. E. HARLOW
Department of Mineral Sciences, American Museum of Natural History, New York, NY 10024-5192, USA

ABSTRACT Jadeitites from Guatemala are found as weathered blocks in tectonized serpentinite in a 15-km zone north of the Motagua Fault Zone. Rock types found with jadeitite include albitites, albite–mica rocks, omphacite/taramitic amphibole-bearing metabasites, chlorite–actinolite schists, talc–carbonate rocks and antigorite schists. In addition to the predominant jadeitic (Jd_{93-100}) pyroxene, common phases in jadeitite include micas (paragonite and/or phengite ± rarer phlogopite), omphacite, albite, titanite ± zircon, apatite and graphite. Conditions of jadeitite formation are 100–400° C, 5–11 kbar with $0.0 > \log_{10}a_{SiO_2} \geqslant 0.7$. Fluid inclusions, coarse textures, vein structures, and rhythmic zoning of pyroxene indicate an aqueuos fluid was involved. Jadeitites are either (1) metasomatic modifications of former felsic-to-pelitic inclusions that have undergone silica depletion plus efficient soda exchange and enrichment, or (2) solution precipitations derived from such a source. The close spatial relationship of faults and shear zones, serpentinites, and jadeitites suggests jadeitites form in a relatively high-*P/T* setting with substantial flow of sodic fluid in a tectonized zone.

Most Guatemalan jadeitites are extensively altered to analcime, albite, taramitic amphibole, (clino)zoisite ± nepheline and preiswerkite. This alteration reflects depressurization ± heating to below the jadeite + fluid = analcime reaction at high a_{Na}. With progressive alteration, analcime and nepheline are replaced by albite; the increase in silica content may result from fluid flowing up a tectonized zone reaching saturation with an albite assemblage. Albitite phases, albite, actinolite, zoisite, ±chlorite, phengite, K-feldspar and quartz, record conditions of *c.* 3–8 kbar at $T < 400°$ C, indicating a clockwise *P–T* trajectory of the blocks.

Barium aluminosilicates—banalsite, celsian, cymrite and hyalophane—are common minor late-stage phases in jadeitites and albite-rich rocks. Barian phengite is common in albite–mica rocks.

Key words: albitite; Guatemala; jadeite; jadeitite; metasomatism; Motagua Fault Zone; **Abbreviations:** these follow Kretz (1983) except as follows: Cel, celsian; Cym, cymrite; Ph, phengite; W, H_2O (fluid).

INTRODUCTION

Jadeitite, a rock composed principally of jadeite, is rare, described from only a handful of localities: the Moguong and Lonkin area of northern Myanmar (formerly Burma: Lacroix, 1930; Chhibber, 1934); Kotaki District and nearby areas, Honshu, Japan (Iwao, 1953; Chihara, 1971); Oosa-cho, Okayama Prefecture, Japan (Kobyashi *et al.*, 1987); Kamuikotan Gorge area, Hokaido, Japan (Takayama, 1986); San Benito County, California (Coleman, 1961); the Pay-Yer massif, Polar Urals, Russia (Morkovkina, 1960); the Borus Mountains; West Sayan, Russia (Dobretsov, 1963, 1984); Northern Near-Balkash region, Kazakhstan (Dobretsov & Ponomareva, 1965); and along the Motagua Fault in Guatemala (Foshag & Leslie, 1955; McBirney *et al.*, 1967; Bosc, 1971; Hammond *et al.*, 1979). Jadeitites occur either as individual tectonic blocks, or as pods, lenses or veins in other blocks within serpentinite or serpentinite–matrix melange. Some interesting aspects of jadeitites are (1) they consist of the presumed high-*P* mineral jadeite, and therefore have an unusual bulk composition (Yoder, 1950; Sobolev, 1949–1960: cited in Dobretsov, 1984); (2) they are associated with ultramafic belts, ophiolites and blueschists and thus with ocean-floor subduction or obduction; (3) they are probably metasomatic, with an origin controlled by the host serpentinite and the active high-*P/T* tectonic setting; and, certainly not least, (4) they are archaeologically and commercially important as jade.

Probably the least well-described occurrence of jadeitites is the one in Guatemala, which is puzzling because the area is reasonably accessible and it is a major source of jadeitite, both archaeologically and commercially (Harlow, 1993). This paper describes the occurrence of jadeitite in the Departments of El Progreso and Zacapa along the Motagua River of Guatemala. The interpretation of jadeitite petrogenesis and its ramifications raise broader questions of collisional processes and fluid–rock interactions. This paper presents a description of the occurrence, the field and textural relationships, and the mineralogy/petrology of the Guatemalan jadeitites and examines the processes of jadeitization and albitization.

REGIONAL GEOLOGY AND FIELD OCCURRENCE

The North American and Caribbean plates abut along the Motagua Valley of Guatemala. It is the junction of two

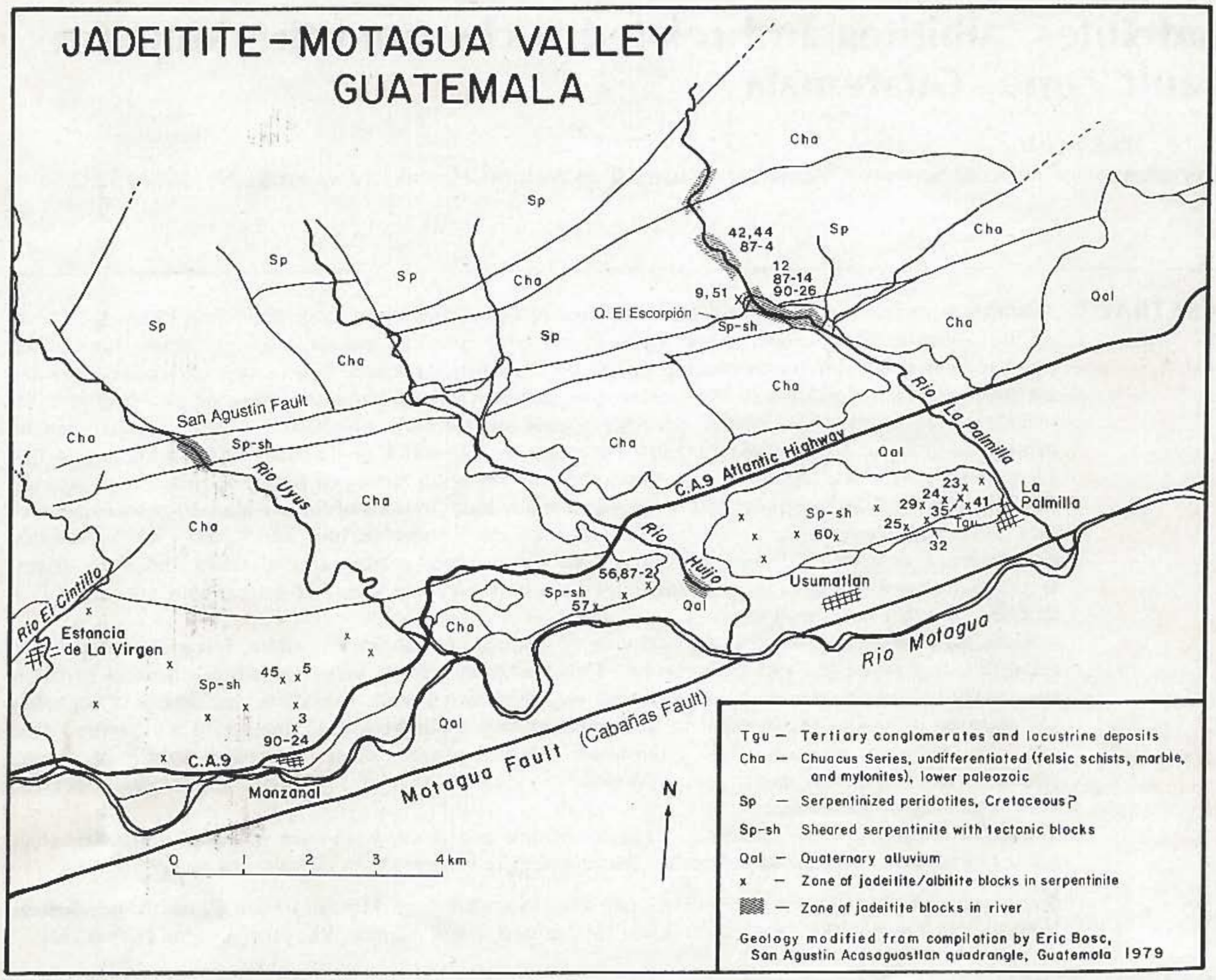

Fig. 1. Location and geological map of jadeitite occurrences in the middle Motagua Valley, Guatemala. Numbered location sites refer to the MVJ classification minus the letters, final site sample number and 84, if from MVJ84 group; e.g. 5 ⇒ MVJ84-5C-1 etc. and 90-24 ⇒ MVJ90-24-1 etc. Imprecise localities are attributed as 'Guat I' in Table 1 but do come from within the study area.

continental blocks, the Maya (or Yucutan) to the north and the Chortis to the south. Portions of an ophiolite complex in the Motagua Valley indicate a major suture. The collision is dated regionally as late Cretaceous (Pindell & Dewey, *1982)* to early Tertiary (Perfit & Heezen, *1978)* and locally as about 68 Ma from $^{40}Ar/^{39}Ar$ dating (Donnelly *et al.*, 1990). The original convergence of the Maya block with the early northern margin of the Caribbean plate has evolved to currently lateral or transform motion (Burke, 1988), with the active tectonic boundary called the Motagua Fault Zone. The recent left-lateral movement (*c.* 100 ka; Schwartz *et al.*, 1979) along this fault zone may extend to *c.* 2000 km offset, according to reconstructions (Anderson & Schmidt, 1983; Wadge & Burke, 1983). Thus, the terranes presently adjacent across the fault zone were in different positions and context at the time of collision. The important fact for the jadeitites and eclogites described by McBirney *et al.* (1967) is that jadeitite is found north of the Motagua Fault Zone and eclogite is found south of it.

In the study area the Motagua Fault Zone is well defined by the active Cabañas Fault and perhaps a conjugate fault, the San Agustin Fault (see Fig. 1). The Sierra de las Minas, the northern boundary of the Motagua Valley, consists of tectonic slices of Palaeozoic schists and marbles of upper greenschist to amphibolite facies and granitoids grouped as the Chuacús Formation by McBirney (1963). Amphibolites and serpentinite of oceanic origin are tectonically interlayered with the Chuacús rocks. A K/Ar isochron age for the metamorphism of the oceanic rocks is *c.* 60 Ma (Bertrand & Vuagnat, 1980). In the study area the terrane is intensely tectonized adjacent to closely spaced faults. Formations are exposed as thin slivers and blocks; this is particularly true of the ultramafic belt.

Reconnaissance of cited occurrences (e.g. Silva, 1970; Bosc, 1971; Hammond *et al.*, 1979) and streams cutting serpentine delimited a *c.* 15-km-long, jadeitite-bearing area (Fig. 1). No comparable rocks were found south of the Motagua River. Jadeitite occurs as boulders (≤3 m in diameter) in some streams, particularly Río La Palmilla.

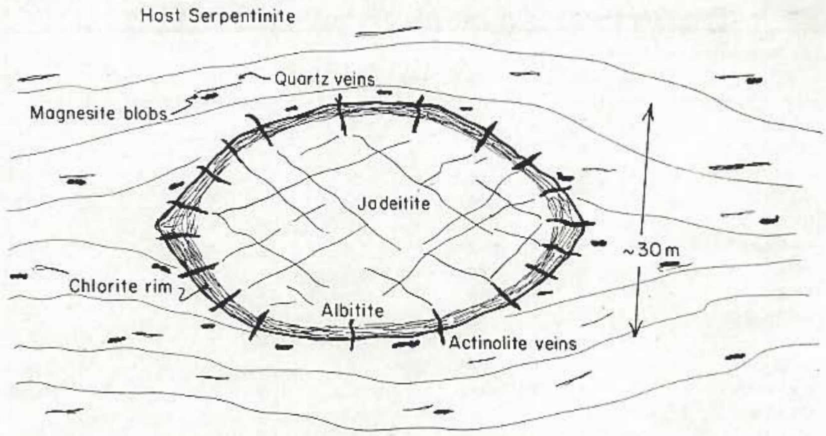

Fig. 2. Schematic diagram of jadeitite/albitite tectonic block in serpentinite-matrix melange.

Jadeitite boulders are conspicuous by their (1) rusty-brown to tan-white cortex, (2) white to medium-green freshly broken surfaces, abundantly provided by blasting by jade entrepreneurs and (3) extraordinary tenacity (boulders deflect hammer blows and rarely break). Jadeitite was not seen weathering from hosting serpentinite. Other stream boulders are serpentinite (antigorite schist), Chuacús granitic gneiss, white to grey Chuacús marbles, metabasite (an amphibole–omphacite rock called black jade) and albitized jadeitite. Bosc (1971) reported jadeitite in Río Uyus (see Fig. 1).

Two areas ≤50 m in diameter are decorated with weathered blocks <2 m across. At MVJ84-5 is an area of albitite blocks; no jadeitite was found here, but small cobbles were found nearby to the south. Silva (1970) noted that jadeitite is scattered throughout this serpentinite body (Fig. 1). Blocks of jadeitite equivalent to those found in Río La Palmilla occur at MVJ84-9 & -51.

In weathered, ochre-earthed, serpentinite hills near the Río Motagua, tan-coloured mounds and noses of hills are littered with fragments and blocks (<0.5 m across) of jadeitite, albitite and metabasite (see Fig. 1). The mounds range in size from a few to c. 50 m in diameter and also contain opal, chalcedony and milky quartz, fragments of deep-green omphacite, chlorite–actinolite rock, mammillary magnesite and weathered serpentinite. Albitite was found in all of the mounds, but jadeitite was rare or absent. Although no bedrock exposures were found, even after excavation (at MVJ84-35), a zoning pattern was (Fig. 2); it consists of exterior serpentinite, a chloritic boundary and an interior mix of fragments of jadeitite and albitite. The chlorite boundary contains areas of talc and is cut by parallel aggregates of acicular actinolite + chlorite ≤1 m long.

JADEITITES AND ALBITITES: TEXTURES AND MINERALOGY

Analytical techniques

Optical and SEM/BSE petrographical and microprobe analyses of thin sections and X-ray diffraction of rock slabs or mineral grains were performed. An automated ARL SEMQ microprobe (with Tracor-Northern TN5400 EDS) was operated at 15 kV, 10–12 nA sample current for Na-bearing or hydrous silicates and 20 kV, 15 nA for oxides and other silicates. Standards included diopside, jadeite, Amelia albite, microcline, Kakanui hornblende, Cape Ann fayalite, chromite, ilmenite, benitoite, celestite, Durango apatite, quartz and corundum. Back-scattered electron (BSE) imaging was carried out on the microprobe and on a Zeiss DSM-950 SEM. X-ray diffraction employed an automated Philips PW1710 diffractometer and Gandolfi cameras using Cu $K\alpha$ radiation. Phase identification was aided with the μPDSM search/match program.

Macroscopic description

Two spatial groupings of jadeitite are manifested. One is near Manzanal (Mzl), near the western limit of the study area, and the other is closer to Río La Palmilla (RLP; Fig. 1). Mzl jadeitites are generally whiter than RLP ones and the former also lack black or dark green minerals. These features relate to differences in composition and phase assemblages described below.

Jadeitite boulders are generally fractured, sheared and altered. Fine-grained jadeitites typically show subtle marbling. Many boulders have an augen-like texture of coarse, fractured, lighter-coloured jadeitite in a matrix of grey albititic rock. Some boulders show a transition from relatively pure, massive jadeitite, through augen texture, to blue–grey or green albitite (Fig. 3). At MVJ84-9, -12 & -51, jadeitite and metabasite blocks are cut by sharply defined, 1–30-cm-wide veins of jadeitite filling brittle fractures. The vein fillings consist of cross-vein, subparallel

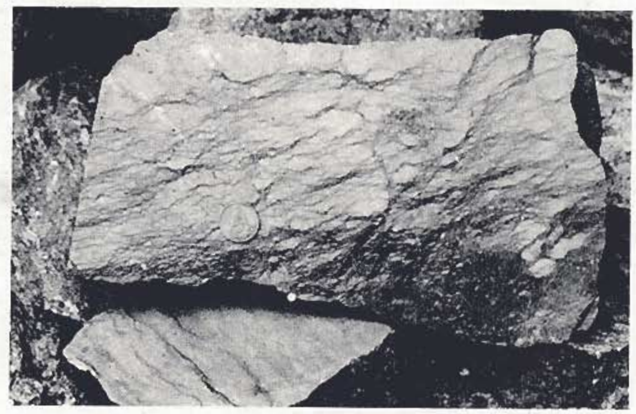

Fig. 3. Transition from jadeitite (upper left, light-coloured zone) through fractured alteration zone to albitite (lower right, dark grey zone) in a sliced boulder at a jade workshop. The coin is 25 mm across.

Table 1. Mineralogy of samples used in this study. Locality Guat. I indicates samples collected by others somewhere within the known field area.

(A) Jadeitites and partially altered jadeitites

	jd	omp	ab	wm	amp	anl	ne	zo	ttn	gph	prs	other	Description	Locality
MVJ84-9B-1	×		×	pg	×	×	×	×			×	apt	Light green & black	Quebrada Escorpión
MVJ84-9C-1	×	×	×	pg	×	×	×	×	×		×	bnl,zr	Light & dark green	Quebrada Escorpión
MVJ84-9C-2	×	×	×	pg	×	×		×	×		?	cc?	Light green	Quebrada Escorpión
MVJ84-9D-1	×		×	pg	×	×	×	×	×	×	×	apt,cnc	Grey–black	Quebrada Escorpión
MVJ84-12-5	×		×	pg	×	×	×	×	×		×	bnl,zr	White & black	Quebrada Escorpión
MVJ84-29-2	×	×	×	pg,phl	×				×	×		zr	Bluish grey	Usumatlán
MVJ84-32-3	×	×	×	pg					×	×	×		Mottled white & grey	La Palmilla
MVJ84-42-1	×		×	pg	×	×	×	×	×		×		Whitish green	Río La Palmilla
MVJ84-42-2	×		×	pg	×	×	×	×			×		White & black	Río La Palmilla
MVJ84-51-3	×	×	×	pg	×			×	×				Light green	Quebrada Escorpión
MVJ84-56-1	×	×	×	pg,ph		×				×		phl,zr	White & grey	Hoyo de las Minas
MVJ-87-8-1	×	×	×	ph,pg		×		×	×			phl,apt,kfs	Mottled white & green	Guat. I
MVJ-87-8-2	×												Light blue–green	Guat. I
MVJ90-24-1	×	×	×	pg,ph		×		×				phl,kfs,cc	Whitish green	Manzanal
MVJ90-24-2	×		×	ph,pg		×						phl,kfs	White	Manzanal
MVJ90-24-3	×	×	×	pg				×				kfs,barite	Light green	Manzanal
MVJ90-26-7	×	×	×	pg	×	×	×	×	×		×	bnl	Dark grey	Río La Palmilla
AMNH 33399	×		×	ph,mu		×							White	Manzanal?
AMNH 45049	×	×	×	pg	×			×			×	cc?	Light green	Guat. I
NMNH 112538-3	×	×	×	ph,pg		×		×				phl,kfs	Light green	Manzanal?
R-1	×	×	×	pg				×	×				Sea foam	Guat. I
R-4	×	×	×	phl					×				Mint	Guat. I
R-6	×	×	×	pg	×				×				Pearl	Guat. I
R-7	×		×	pg	×	×		×					Forest fog	Guat. I
R-11	×		×	pg		×		×	×		×	apt	Olmec blue	Guat. I
R-12	×	×	×	phl,pg	×	×	×	×			×	zr,zeo	Dusk	Guat. I
R-13	×	×	×	pg							×		Foliage	Guat. I
R-15	ko_6	×	×	pg	×	×	×						Light emerald-green	nr Río La Palmilla

(B) Pyroxenites (omphacitites) and metabasites

	jd	omp	cm	ab	wm	amp	czo	ttn	chl	zr	gph	grs	other	Description	Locality
Omphacite															
MVJ84-41-4		ko_37	×	×					×						
MVJ84-44-2		×		×		×		×					apt,cpy	Dark green	La Palmilla
MVJ84-51-2	×	×		×		×		×		×	?		bio	Green/black	Río La Palmilla
NHMLAC 20368	×	×		×	pg/phl			×	×	×	×		hyl	Dark green	Río La Palmilla
R-10		×		×	phl				×		×		kfs,cel	Dark green	Guat I.
Metabasite															
MVJ84-23-1		×		×		×	×	×				×	apt,rut,ilm	Black	La Palmilla
MVJ84-51-1		×		×		×		×		×		×		Black	Quebrada Escorpión
MVJ87-14-1		×		×		×	×	×		×		×	bio	Black	Río La Palmilla
NHMLAC 20370		×		×		×	×	×				×		Black	Río La Palmilla

(C) Albitites and highly altered jadeitites

	cpx	ab	wm	amp	anl	qtz	zo	ttn	chl	zr	other	Description	Locality
MVJ84-5C-1	di	×	ph	tr		×			×	×		Whitish grey–green	Manzanal
MVJ84-12-1	om	×		ftar	×		×	×			apt,grs	Whitish blue–green	Río La Palmilla
MVJ84-24-2	di	×		act		×	×	×	×	×	ver	White	Usumatlán
MVJ84-25-1	di	×				×				×	magnetite	Mottled white & green	Usumatlán
MVJ84-57-1		×		act				×			ver?	Light green	Huijó
MVJ84-60-1	di/om	×				×		×	?		hematite	Light green	Usumatlán

(D) Albite–mica rocks

	cpx	ab	kfs	bas	wm	amp	qtz	zo	ttn	chl	other	Description	Locality
MVJ84-3-2		×		cym	ph		?			×	apt	Tan white	Manzanal
MVJ84-23-2		×	×	cel	ph/mu			×	×	×	barite,hyl	Grey–brown	La Palmilla
MVJ84-25-2		×	×	cel	ph/pg			×		×			Usumatlán
MVJ84-29-1		×	×	cel	ph/phl			×		×	,hyl	Tan brown	Usumatlán
MVJ84-45-1		×	×	cel	ph	act			×	×		Light green	Manzanal
MVJ87-2-1		×			ph		×	×				Tan white	Hoyo de las Minas
MVJ87-4-1	di	×					×	×	×		gph,zr	Dark grey	Río La Palmilla

* AMNH, American Museum of Natural History; NHMLAC, Natural History Museum of Los Angeles County; NMNH, National Museum of Natural History; R, Ridinger, Jade S.A.; MVJ, author's field study; ab, albite; amp, amphibole (act, actinolite; ftar, ferroan taramite; tr, tremolite); anl; analcime; apt, apatite; bas, Ba-silicates (cel, celsian; cym, cymrite); bio, biotite; bnl; banalsite; cc, calcite/aragonite; chl, chlorite; cm, chromite; cnc, cancrinite; cpx, clinopyroxene (ag, augite; di, diopside; om, omphacite); cpy, chalcopyrite; czo, clinozoisite; gph, graphite; grs, grossular; hyl, hyalophane; ilm, ilmenite; jd, jadeite; ko, kosmochlor; kfs, K-feldspar; mu, muscovite; ne, nepheline; omp, omphacite; phl, phlogopite; prs, preiswerkite; qtz, quartz; rut, rutile; ttn, titanite; ver, vermiculite; wm, white mica (pg, paragonite; ph, phengite); zeo, zeolite; zo, zoisite; zr, zircon.

pyroxene crystals intergrown with paragonite and lesser amounts of omphacite, albite and zoisite. Boulders do not show clear evidence of core–rim relationships, which indicates they are not complete samples of a serpentinite-block package.

Many light-green, fine-grained rocks that look like jade are, in fact, albitite. In serpentinite, green albitites occur with grey albite–mica rocks. Albitite and albite–mica rock textures vary from coarse to fine grained and from arenaceous-looking to mylonitic.

Microscopic textures and mineralogy

Table 1 lists specimen numbers, mineralogy, colour and location for the samples examined petrographically. Samples are grouped by petrological type as described in the following text. Some were obtained from museum and other collections, so locality information can be vague. A paragenetic sequence based on the textural observations is presented in Table 2.

Jadeitites

These rocks consist of >90% (by volume) jadeititic pyroxene with minor secondary minerals. However, many jadeititic rocks contain <50% pyroxene and substantial quantities of alteration minerals, primarily albite.

Jadeitites display diverse microscopic textures. Microcrystalline varieties of jadeitite consist of either felted masses or sheared, granular compact aggregates of submillimetre-sized (to even micrometre-sized) pyroxene crystals with minor white mica and rare albite and titanite. Coarser-grained rocks (0.5–10 mm) are dominated by irregular to subhedral jadeite intergrown with or containing inclusions of white mica, minor to trace albite and, in some samples, apatite, titanite or zircon (Fig. 4a). In vein fillings, pyroxene crystals can exceed 15 cm. In thin section, however, such crystals are broken into smaller grains (<3 cm) and display mosaic texture. Most jadeite crystals from veins manifest rhythmic zoning with bands 10 μm to 1 mm thick. Some zoned grains of vein jadeite terminate with crystal faces in cavities filled with analcime (Fig. 4b). Small (*c.* 100–10 μm) two-phase (gas–liquid) fluid inclusions occur in coarse jadeite grains as clusters in crystal cores and decorating growth zones and healed fractures. Fluid inclusions typically are irregularly shaped but elongated parallel to the jadeite *c*-axis.

Table 2. Inferred paragenetic sequence in jadeitite–albitite formation.

Crystallizing stable (—) or metastable (- - -) phase	Jadeitite	Alteration/ albitization	Albitites
Jadeite	—— - - -	- - -	
Calcic clinopyroxene	Jd_{50}	—— Jd_{30}	—— Di_{90}
Albite	——	——	——
Paragonite	——	- - -	
Phengite	——	—- - - ?GAP? - -	——
Phlogopite	? ——	——	——
Preiswerkite		—— - - - -	
Chlorite	? - -	- - - ? ——	——
Titanite	- - - - - - ? - - - ——	——	——
(Clino)Zoisite	? ——	——	——
Analcime		—— - - - - -	
Nepheline		—— - - - - -	
Amphibole	Taramite	—- - - ?GAP?	- - - —— Tr_{90}
Banalsite		—— - - -	
Celsian			——
Cymrite			——
K-feldspar			——
Quartz		——	——

In many coarser-grained jadeitites, jadeite grains have clean rims but display cores with numerous inclusions of albite, white mica or (clino)zoisite that are <100 μm in size (Fig. 4c,d). Such inclusions in RLP jadeitites also include rare amphibole, nepheline, preiswerkite (an Na–Mg trioctahedral mica) and analcime. Inclusions are elongated along the *c*-axis of jadeite. With increasing grain size or evidence of deformation, jadeite grains manifest a thin analcime rim (Fig. 4d) and are separated by a matrix of alteration minerals described below.

In RLP jadeitites, omphacite occurs in some crack and cavity fillings as wheat-sheaf intergrowths and also forms overgrowths on jadeite, particularly on pyramidal faces. Where such overgrowths are more than 100 μm thick, the overgrowth can consist of acicular aggregates of omphacite extending parallel to the *c* crystallographic axis of the host. In blotchy green jadeitites, omphacite forms rhythmically zoned radiating clusters intergrown with albite and/or chlorite.

White mica in jadeitites is found as interstitial grains or as inclusions in jadeite. All RLP jadeitites contain only paragonite. In coarse jadeitite veins paragonite forms books ≤ 1 cm thick and ≤4 cm in diameter. Jadeitite samples from further west contain paragonite, phengitic muscovite and/or phlogopite. A few samples contain three micas, but mica relationships are difficult to interpret because of alteration. Rare grains of muscovite are found as inclusions in jadeite that coexists with phengite.

Most other minerals are very minor in abundance in unaltered jadeitites. Albite occurs rarely as large discrete grains but commonly as vein/crack and intergranular fillings. Albite is rarely twinned. Titanite is found in some jadeitites as corroded dismembered relics < 1 mm in size but also as small intergranular grains (subhedral to angular), usually associated with albite. Apatite is common but minor, except in sample MVJ84-9D-1 which contains *c.* 5% as vein-like aggregates of apatite grains. Zircon is a scattered trace phase as small rounded to subhedral grains. Chlorite forms minor intergranular selvages in omphacite clots.

Some jadeitites, mainly near RLP, are coloured grey to nearly black by minute (<50 μm in maximum dimension) ball-like clusters of graphite in jadeite and albite grains or in intergranular fillings. Carbon count rates on the microprobe from graphite clusters approach those for pure carbon, but accurate analyses were not possible.

Quartz was not found in any jadeite-bearing sample, contradicting McBirney *et al.* (1967). Duncan (1986) reported lawsonite and prehnite in jadeite-bearing rocks; neither was identified in the samples reported here.

Alteration textures in jadeitite

Alteration is a common feature of most jadeitites. Replacement of jadeite varies from minor, along grain boundaries (described above), to nearly complete. In RLP specimens fractures in jadeite crystals and grain boundaries are filled with anastamosing or vermicular "cross-crack" intergrowths of albite + analcime (Fig. 5a). Textures consist of reticulated or idiomorphic albite grains in analcime, with the grains coarsening away from the contact with jadeite. In one sample (R-12), a region between jadeite and analcime consists of a vermicular intergrowth of nepheline + albite. Within the vermicular networks, epitaxial prismatic blue amphiboles extend parallel to the *c*-axis of the replaced pyroxene (Fig. 5a). Some zones between jadeite grains contain blebby intergrowths of analcime + albite with interspersed euhedral to skeletal titanite, zoisite and, in RLP samples, amphibole and preiswerkite grains.

In extensively altered jadeitite, analcime–albite intergrowths are less common or absent far from jadeite grains and are replaced by granular albite. Sometimes isolated, faceted jadeite grains and larger amphibole crystals or rosettes (<4 mm across) occur in a matrix of albite. The albite matrix also contains euhedral (clino)zoisite grains (micrometre- to millimetre-sized) ± smaller grains of titanite, apatite, calcite/aragonite and zircon.

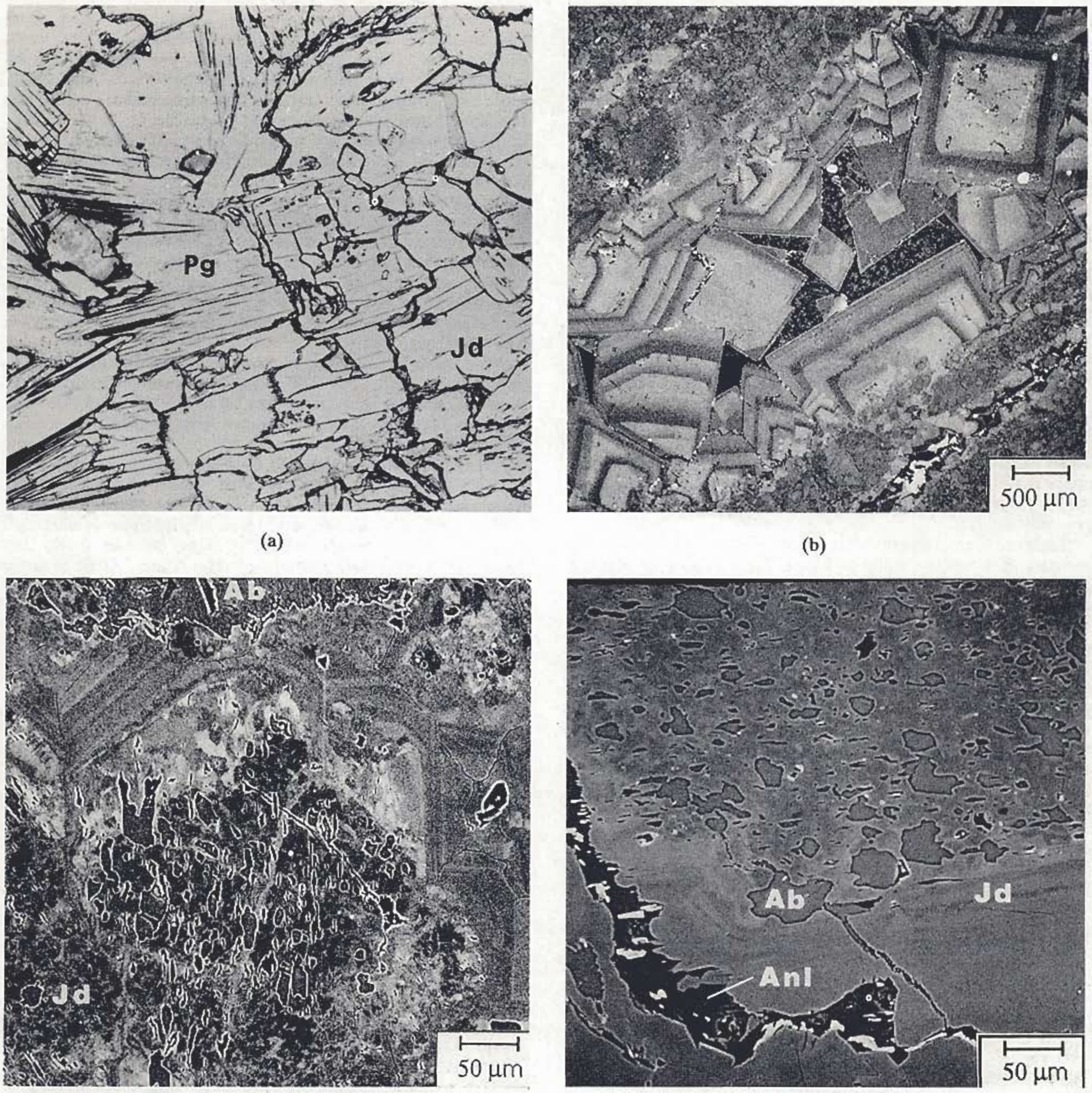

(a) (b) (c) (d)

Fig. 4. Thin-section photomicrographs of jadeitite. (a) Medium-grained jadeitite texture with coexisting jadeite and paragonite grains. A thin selvage of analcime covers many jadeite grain boundaries (sample AMNH 33399; plane-polarized-light, width of view is 2 mm). (b) BSE image of rhythmically zoned jadeite crystals in vein-growth jadeitite (sample MVJ84-9C-2). (c) BSE image of jadeite grain with numerous core inclusions and zoned rim from a partially retrograded jadeitite (sample MVJ84-9D-1). The host jadeite (mottled grey) is irregularly zoned (brighter areas have higher diopside content) in the interior with many inclusions of albite (grey) and voids (black). The jadeite rim is rhythmically zoned. The vein filling at top shows albite. (d) BSE image of jadeite with core albite inclusions, clear rim and analcime along the grain boundary with included idiomorphic amphibole grains (sample MVJ84-9D1).

Mica alteration textures vary with mica composition. In RLP samples, paragonite grains are usually surrounded by a band of granular clouded nepheline, filled with micrometre-sized inclusions of paragonite, and rimmed by clear nepheline (Fig. 5b). Nepheline is usually in contact with analcime rather than albite. Small grains of paragonite are rarely surrounded by clear banalsite (an Na–Ba feldspar relative), but banalsite and nepheline are not found together. Small fragments of paragonite ± preiswerkite are seen in some cores of euhedral zoisite. Preiswerkite also occurs as small platy blebs and irregularly shaped grains in albite. Phlogopite in altered zones looks pitted and is visibly intergrown with chlorite. Phengite is pitted in some altered samples but appears fresh in others. In several altered jadeitites phengite grains have barian overgrowths.

Altered Mzl jadeitites contrast with RLP jadeitites by having less dramatic textures and somewhat different mineralogy. In the

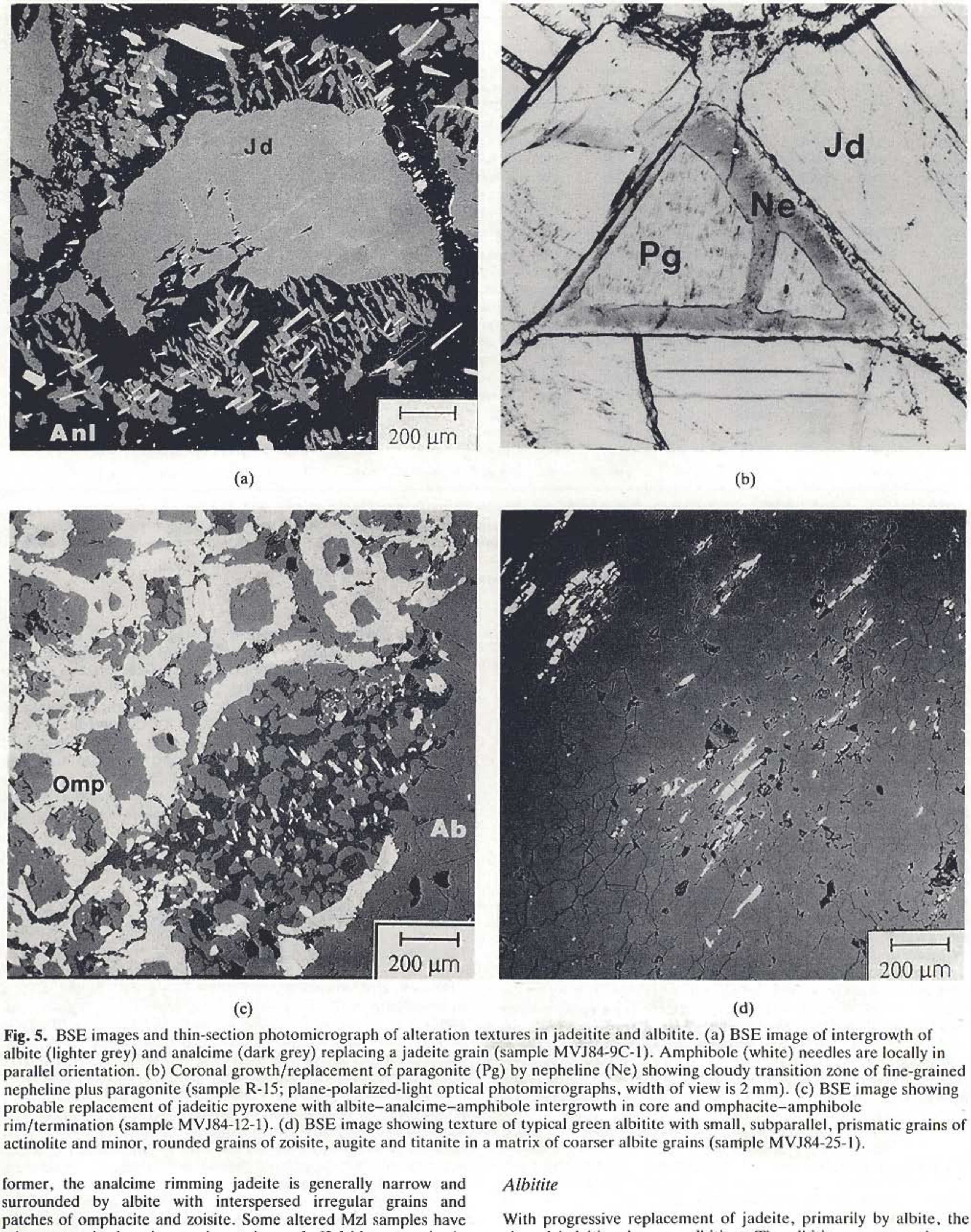

Fig. 5. BSE images and thin-section photomicrograph of alteration textures in jadeitite and albitite. (a) BSE image of intergrowth of albite (lighter grey) and analcime (dark grey) replacing a jadeite grain (sample MVJ84-9C-1). Amphibole (white) needles are locally in parallel orientation. (b) Coronal growth/replacement of paragonite (Pg) by nepheline (Ne) showing cloudy transition zone of fine-grained nepheline plus paragonite (sample R-15; plane-polarized-light optical photomicrographs, width of view is 2 mm). (c) BSE image showing probable replacement of jadeitic pyroxene with albite–analcime–amphibole intergrowth in core and omphacite–amphibole rim/termination (sample MVJ84-12-1). (d) BSE image showing texture of typical green albitite with small, subparallel, prismatic grains of actinolite and minor, rounded grains of zoisite, augite and titanite in a matrix of coarser albite grains (sample MVJ84-25-1).

former, the analcime rimming jadeite is generally narrow and surrounded by albite with interspersed irregular grains and patches of omphacite and zoisite. Some altered Mzl samples have micrometre-sized veins and patches of K-feldspar and, in MVJ90-24-3, barite. Altered jadeitites from Manzanal lack vermicular textures, amphibole, preiswerkite and nepheline.

Albitite

With progressive replacement of jadeite, primarily by albite, the altered jadeitites become albitites. The albitites are a continuum of albite-dominant rocks with strong affinities to jadeitite alteration. The mineralogy of albitites resembles the alteration

Table 3. Representative microprobe analyses of pyroxenes (6 O basis).

	1	2	3	4	5	6	7	8	9	10	11	12	13	14
SiO_2	60.42	58.77	59.42	57.56	59.06	59.93	58.75	59.68	54.99	54.92	55.33	55.28	53.80	53.10
TiO_2	0.00	0.00	0.04	0.07	0.00	0.04	0.01	0.16	0.06	0.05	0.13	0.05	0.04	0.03
Al_2O_3	25.39	21.07	24.15	12.10	25.46	23.84	20.08	18.65	5.80	10.15	10.16	3.29	3.28	2.17
Cr_2O_3	—	0.00	0.00	0.03	—	—	0.01	1.93	3.71	0.00	0.00	—	—	0.56
$Fe_2O_3^*$	0.12	1.42	0.71	2.38	0.22	1.28	2.15	1.58	4.32	1.96	2.14	5.95	2.10	0.93
FeO	0.12	0.00	0.00	1.68	0.00	0.00	0.00	0.00	1.08	8.92	7.83	1.53	3.21	7.93
MnO	0.02	0.17	0.00	0.20	0.05	0.04	0.09	0.03	0.00	0.34	0.12	0.32	0.27	0.27
MgO	0.06	1.84	0.45	7.31	0.04	0.57	2.34	1.88	9.08	4.51	5.25	11.73	13.11	11.30
CaO	0.20	2.77	0.76	12.13	0.13	1.01	3.73	3.25	13.77	12.70	12.93	19.06	20.68	21.44
Na_2O	15.45	13.51	15.01	8.10	15.50	15.06	13.02	13.06	6.35	6.79	7.04	4.20	2.57	1.77
Total	101.79	99.55	100.54	101.56	100.45	101.78	100.18	100.22	99.17	100.36	100.92	101.41	99.06	99.50
Si	2.00	2.01	2.00	2.00	1.98	2.00	2.01	2.04	2.00	2.00	2.00	1.99	1.98	1.99
Ti	0.000	0.000	0.001	0.002	0.000	0.001	0.000	0.004	0.002	0.001	0.003	0.001	0.001	0.001
Al	0.99	0.85	0.96	0.50	1.01	0.93	0.81	0.75	0.25	0.44	0.43	0.14	0.14	0.096
Cr	—	0.000	0.000	0.001	—	—	0.000	0.052	0.11	0.000	0.000	—	—	0.017
Fe^{3+*}	0.003	0.037	0.018	0.062	0.006	0.032	0.055	0.041	0.12	0.054	0.058	0.16	0.058	0.026
Fe^{2+}	0.003	0.000	0.000	0.049	0.000	0.000	0.000	0.000	0.033	0.27	0.24	0.046	0.099	0.25
Mn	0.000	0.005	0.000	0.006	0.001	0.001	0.003	0.001	0.000	0.010	0.004	0.010	0.008	0.008
Mg	0.003	0.094	0.023	0.38	0.002	0.029	0.12	0.095	0.49	0.25	0.28	0.63	0.72	0.63
Ca	0.007	0.10	0.027	0.45	0.005	0.036	0.14	0.12	0.54	0.50	0.50	0.73	0.82	0.86
Na	0.99	0.90	0.98	0.55	1.01	0.97	0.86	0.87	0.45	0.48	0.49	0.29	0.18	0.13
Total	4.00	3.99	4.00	3.99	4.02	4.00	3.99	3.97	3.99	3.99	4.00	4.00	4.01	4.00

(1) Jadeite in white jadeitite, AMNH 33399; (2–3) adjacent spots in jadeite grain, R-12; (4) overgrowth omphacite on same grain, R-12; (5) in core zone of jadeite grain, MVJ84-9D-1; (6) rim, same grain as (5), MVJ84-9D-1; (7) an impure jadeite from a green jadeitite, R-13; (8) slightly chromian jadeite, R-15; (9) chromian omphacite, MVJ-41-4, omphacite; (10) omphacite, NHMLAC 20370, metabasite; (11) omphacite, MVJ84-51-1, metabasite; (12) aegirine–augite, MVJ84-60-1, albitite; (13) diopside, MVJ84-5C-1, albitite; (14) diopside, MVJ84-24-2, albitite.

* Fe^{3+} estimated by cation sum and charge balancing. Pyroxene nomenclature after Morimoto *et al.* (1988).

assemblage in jadeitites: calcic clinopyroxene, amphibole, zoisite, titanite, and rarely apatite, zircon, chlorite and grossular in a matrix of rarely twinned albite. Quartz is generally absent in albitites that contain omphacite but is minor to abundant in other albitites as <10-μm blebs in albite or as interstitial grains 10 μm to 2 mm in size. Analcime is rare or absent and does not coexist with quartz.

An important characteristic of albitites is the texture and mineralogy related to alteration of jadeitic pyroxene. In albitites, omphacite grains resemble pyramidal terminations of relict pyroxene grains. Such "pyroxene" interiors are occupied by albite and amphibole (Fig. 5c). Aegirine augite and diopside are found as clustered or isolated blebs in albitites. Amphibole changes from taramite in alteration-textured rocks towards or to actinolite in quartz-bearing albitite. The relative amounts of clinopyroxene and amphibole in the albitites are controlled by the composition of the original jadeitite; the more Fe-rich the original jadeitite pyroxene, the greater abundance of Fe-rich amphibole and secondary pyroxene in the albitite.

Microscopic evidence of deformation in the albitites consists of opening of cleavage in albite, reducing grain size to a mylonitic texture, and breaking up of relict replacement textures to an even distribution of blebby grains in an albite matrix (Fig. 5d). In albitites that lack replacement textures, the amphibole is actinolite rather than a sodic calcic amphibole and the pyroxene is aegirine augite or diopside rather than omphacite. Thus, deformational homogenization of texture is correlated with compositional change.

Albite–mica rock

Albite–mica rocks do not manifest replacement textures of jadeitite and generally do not contain sufficient albite to be labelled albitites. Albite–mica rocks have a granoblastic texture of millimetre-sized grains of intergrown albite, phengitic muscovite ± minor prismatic actinolite with rare blebs of diopsidic pyroxene, quartz, apatite and/or dolomite. Most of these rocks contain irregular, micrometre- to millimetre-sized grains of celsian or sheath-like to ball-like clusters of platy cymrite, zoned barian phengite ± trace K-feldspar, hyalophane and barite. The Ba zoning of phengite can be irregular but the highest Ba content is in rims or small interstitial grains (Table 4). Clinochlore is found in grain-boundary crevices and interlayered in phengite. K-feldspar occurs as blebs in albite and in small late-stage fractures associated with celsian and hyalophane. One micaceous albite, MVJ84-29-1, manifested phengite replacement of zoisite and may be related to sample MVJ87-4-1, which consists of albite and zoisite.

OTHER ASSOCIATED ROCKS

Omphacite–amphibole rock

These fine-grained dark-green to black metabasites usually have a homogeneous texture, although many blocks are foliated with amphibole prisms lying in the foliation plane. Veins in brittle fractures are filled with dark-green omphacite, greenish jadeitite (jadeite ± mica) or orange–brown grossular with inclusions of black amphibole. In thin section, the rock shows a fine- to medium-grained (10 μm to 1 mm), mesh-textured intergrowth of roughly equal proportions of taramite–ferroan pargasite and ferroan omphacite plus minor amounts of corroded titanite and interstitial fillings of albite. In the massive amphibole–pyroxene intergrowths, the amphibole has a mosaic texture with very irregular outlines, and it may be twinned. Clinozoisite is generally minor, as small rounded to subhedral grains, but may comprise 20% (modal) as grain clusters and larger grains. Grossular forms small veins or cavity fillings enclosing small euhedral amphibole crystals. No eclogitic rocks, *sensu stricto*, have been identified in the jadeitite-bearing terrane.

Table 4. Representative microprobe analyses of micas (22 O basis).

	1	2	3	4	5	6	7	8	9	10	11	12	13	14
SiO_2	45.75	29.65	29.93	50.99	51.83	37.55	45.53	41.83	49.90	48.03	46.44	52.15	52.49	35.58
TiO_2	0.03	0.00	0.00	0.10	0.07	0.17	0.02	0.17	0.19	0.21	0.02	0.04	0.14	0.86
Al_2O_3	38.75	37.11	37.17	28.27	26.75	23.32	40.56	33.18	28.65	30.92	40.49	25.58	25.35	15.42
Fe_2O_3*	0.28	0.00	0.00	0.00	0.00	0.00	0.00	0.00	0.00	0.00	0.00	0.00	0.00	0.00
FeO	0.00	4.41	8.03	0.57	1.24	4.00	0.02	1.08	1.48	1.41	0.42	1.30	1.13	20.76
MnO	—	0.21	0.12	0.00	0.07	0.48	0.04	0.01	—	—	—	—	0.01	0.26
ZnO	—	—	—	0.07	0.00	0.05	0.00	0.00	—	—	—	—	—	—
MgO	0.29	16.36	13.90	3.46	4.03	19.99	0.13	2.48	3.90	2.80	0.38	4.52	4.93	12.64
CaO	0.20	0.05	0.06	0.01	0.00	0.16	0.31	0.04	0.02	0.02	0.21	0.03	0.01	0.07
Na_2O	7.18	7.46	7.32	0.56	0.33	0.52	6.75	0.97	0.28	0.50	5.82	0.33	0.07	0.66
K_2O	0.79	0.24	0.26	10.17	9.69	9.17	0.61	7.08	10.27	9.58	1.52	11.10	10.68	8.85
BaO	0.11	0.00	—	0.44	2.06	0.35	0.00	7.26	1.31	4.14	0.25	0.59	0.80	—
F†	—	—	—	0.04	0.06	0.00	0.09	0.00	—	—	—	—	—	—
Total	93.60	95.49	96.79	94.69	96.13	95.77	94.06	94.10	96.01	97.60	95.55	95.64	95.62	95.11
Si	5.97	4.06	4.10	6.80	6.89	5.27	5.88	5.92	6.65	6.42	5.93	6.95	6.98	5.49
Al^{IV}	2.03	3.94	3.90	1.20	1.11	2.73	2.12	2.08	1.35	1.58	2.07	1.05	1.02	2.51
Ti	0.002	0.000	0.000	0.010	0.007	0.018	0.002	0.018	0.019	0.021	0.001	0.004	0.014	0.10
Al^{VI}	3.93	2.05	2.11	3.24	3.08	1.12	4.06	3.45	3.15	3.29	4.02	2.97	2.95	0.30
Fe^{3+}*	0.027	0.000	0.000	0.000	0.000	0.000	0.000	0.000	0.000	0.000	0.000	0.000	0.000	0.000
Fe^{2+}	0.000	0.51	0.92	0.063	0.14	0.47	0.002	0.13	0.17	0.16	0.045	0.15	0.13	2.68
Mn	—	0.024	0.014	0.000	0.008	0.057	0.004	0.001	—	—	—	—	0.001	0.035
Zn	—	—	—	0.007	0.000	0.005	0.000	0.000	—	—	—	—	—	—
Mg	0.057	3.34	2.84	0.69	0.80	4.18	0.024	0.52	0.78	0.56	0.073	0.90	0.98	2.91
ΣR^{VI}	4.01	5.92	5.89	4.01	4.03	5.85	4.09	4.11	4.11	4.03	4.14	4.01	4.07	6.02
Ca	0.027	0.008	0.009	0.002	0.001	0.024	0.043	0.005	0.002	0.003	0.029	0.004	0.002	0.012
Na	1.82	1.98	1.95	0.15	0.086	0.14	1.69	0.27	0.073	0.13	1.44	0.085	0.017	0.20
K	0.13	0.041	0.045	1.73	1.64	1.64	0.10	1.28	1.75	1.63	0.25	1.89	1.81	1.74
Ba	0.006	0.000	—	0.023	0.11	0.019	0.000	0.40	0.069	0.22	0.012	0.031	0.042	—
ΣR^{XII}	1.99	2.03	2.01	1.90	1.84	1.83	1.83	1.95	1.89	1.98	1.80	2.01	1.87	1.95
Total	13.99	15.95	15.89	13.91	13.87	15.68	13.93	14.07	14.00	14.01	13.87	14.02	13.94	15.98
F				0.017	0.027	0.000	0.035	0.000						

(1) Paragonite, MVJ84-9C-1, jadeitite (+ SrO = 0.23, Sr = 0.015); (2) preiswerkite, MVJ84-9C-1, jadeitite; (3) preiswerkite, MVJ84-9B-1, jadeitite; (4) phengite, MVJ90-24-2, jadeitite; (5) barian phengite, MVJ90-24-2, jadeitite; (6) phlogopite, MVJ90-24-2, jadeitite; (7) paragonite MVJ90-24-2, jadeitite; (8) barian phengite, MVJ84-29-1, albite–mica rock; (9) phengite, MVJ84-29-1, albite–mica rock; (10) barian phengite, MVJ84-25-2, albite–mica rock; (11) paragonite, MVJ84-25-2, albite–mica rock; (12) phengite, MVJ84-3-2, albite–mica rock w/cymrite; (13) phengite, MVJ84-5C-1, albitite; (14) biotite, MVJ84-51-2, pyroxene vein in metabasite.

* Fe^{3+} estimated by cation sum and charge balancing.

† Cl found in only trace amounts in the same analyses as for F.

Omphacitite

Found with jadeitite are fist-sized or smaller green rocks that consist almost entirely of omphacite intergrowths with very minor albite, chlorite ± phlogopite, paragonite, and late-stage K-feldspar, hyalophane and celsian. The clots of omphacite in jadeitite are similar to these small isolated omphacitites. Some omphacite aggregates have a conspicuous emerald-green colour and contain small corroded chromites (usually < 20 μm) surrounded by a region of Cr-rich omphacite (Harlow & Olds, 1987).

Chlorite–actinolite rock

At the boundary between tectonic inclusions and serpentinite are long, parallel clusters (up to 25 cm) of actinolite prisms (cross-sections < 4 mm) with interstitial chlorite plates (≤1 mm thick). In the float around exposed tectonic inclusions, cobbles of this coarse-textured assemblage are found, as are pieces of a fine-grained version in felted masses (amphibole prisms < 200 μm by < c. 3 mm) ± schistose foliation. Magnetite or chromite and possibly vermiculite are found as trace phases.

Talc–carbonate rock

A talc–carbonate rock is associated with some albitites. This tan to white rock consists of a fine-grained, white phyllosilicate matrix surrounding centimetre-sized clots of tan carbonate. The matrix consists of undulating intergrowths of chlorite and talc and millimetre-sized fan-shaped sprays of talc. The carbonate is mostly millimetre-sized ferroan magnesite with fine-grained interstitial dolomite. Rare clumps of micrometre-sized iron oxides are found adjacent to the carbonate grains.

Antigorite rock

Antigorite rock occurs as stream boulders and as blocks in less competent serpentinite. Most are non-foliated, but some are schistose. Antigorite grains occur as subparallel plate bundles that form a mosaic with grain sizes from about 10 μm to 1 mm. There are sparse grains of magnetite or chromite; in a chromite-bearing sample, the spinels are surrounded by talc. Some vein fillings of magnesite are preserved.

MINERAL CHEMISTRY

Pyroxene compositions (Table 3) are well described by quadrilateral and sodic pyroxene components with little evidence of Al^{IV} or vacancies. White jadeitites contain essentially end-member jadeite, e.g. AMNH 33399 (Jd_{100}), with minor, if any, Fe-poor omphacite, e.g. $Jd_{53}Di_{40}Ac_6Hd_1$ in MVJ90-24-1. Greener jadeitites contain jadeite with up to about 20 mol% other components (analysis 7, Table 3) and, usually, omphacite. The Fe content of most jadeite ranges from 0.01 to 0.04 cations per 6 O but in some samples exceeds 0.1 cations, whereas the Fe content of most omphacite is 2–4 times (in cations) that of coexisting jadeite. The agent of emerald-green jade colouring is Cr^{3+} as kosmochlor component (Harlow & Olds, 1987). In samples with chromian jadeite or omphacite, Fe content—probably as Fe^{3+}—(analyses 8 & 9, Table 3) is also enriched, although the reverse is not generally true.

Jadeite and omphacite grains are either irregularly zoned or rhythmically banded. In most samples, the range of pyroxene compositions is only 5–10 mol% Jd, such as Jd_{95-99} in jadeite and Jd_{41-50} in omphacite in sample AMNH 45049. The greatest compositional range is in rhythmically zoned jadeite from coarse veins, e.g. $Jd_{99}Ac_1$ to $Jd_{83}Di_{14}Ac_3$ in MVJ84-9C-2. Individual bands in rhythmic zoning (e.g. Fig. 5c) start relatively Jd-rich and decrease in jadeite content as they grow, varying from 2 to 10% Jd content in a single band. The cores of most inclusion-rich jadeite grains are irregularly zoned, and there is no consistent compositional relationship between cores and rims (analyses 2 & 3, 5 & 6, Table 3).

Carpenter (1979) noted a break in pyroxene compositions from diopsidic jadeite to jadeitic omphacite in Guatemalan jadeitite, a gap between Jd_{90} and Jd_{55} (Table 3, Fig. 6). The exact compositional break varies somewhat from specimen to specimen. A gap is also found between the compositions of augitic pyroxene in albitite and the cluster of compositions of omphacite from other rocks. Alteration leads to a reduction in jadeite content (Fig. 6) of calcic Cpx, ultimately yielding diopside in albitite MVJ84-24-2. The Fe contents of the diopsidic pyroxene in the albitites are dispersed. The higher Fe content of omphacite from metabasites than from jadeitites or omphacitites is consistent with omphacites having an affinity with jadeitites.

White mica compositions (Table 4) generally conform to known relationships for paragonite and phengite (e.g. see Guidotti, 1984). Values of K/(K + Na) (KKNa) for paragonite vary from *c*. 0.02 to 0.08 in all samples; paragonite contains significant Ca, minor Fe and Mg and, in some cases, minor Ba. The Si in phengites ranges from 6.4 to 7 cations per 22 O in jadeitites and from 6.3 to 6.9 in albitites. The range of $Mg/(Mg + Fe_{Total})$ (MMF) for phengite is 0.6–0.8 in albitites and up to 0.9 in jadeitites. The average KKNa value for phengite is *c*. 0.94 in jadeitites, with up to 5% variation in any sample, and is 0.88–0.97 in albitites. Examination by XRD yields only the $2M_1$ polymorph of paragonite and phengite.

Barium contents of phengites in both jadeitites and albitites reach values up to 0.10 Ba cations per 22 O, comparable to those reported by Ernst (1963) in phengites from two glaucophane schists. However, phengites in albitites with celsian or cymrite contain up to 0.40 Ba cations (analysis 8, Table 4). The compositional variations are most consistent with a $Ba^{XII} + Al^{XII} \rightleftharpoons K^{XII} + Si^{IV}$ substitution mechanism, typically cited for Ba-enriched phlogopite (e.g. Bol *et al.*, 1989; Pan & Fleet, 1991). This substitution decreases the number of Si atoms per formula unit and thus produces an apparent decrease in the celadonite component of the phengites.

Preiswerkite was first reported as a reaction rind around pargasite within rodingite from the Alpine Geisspfad complex (Keusen & Peters, 1980) and subsequently found in retrogressed eclogites from Switzerland (Meyer, 1983), France (Goddard & Smith, 1984) and Norway (Tlili *et al.*, 1989); Guatemalan jadeitites constitute the fifth occurrence of this mica. The structural formula for preiswerkite in altered jadeitites is (average of many microprobe analyses; OH balanced to cation totals and 10 O) $(Na_{0.97}K_{0.03})(Mg_{1.5}Al_{1.0}Fe^{2+}_{0.4})(Al_{1.9}Si_{2.1})O_{10}(OH)_{1.9}$. The compositions are more Fe-rich in some cases here (MMF = 0.75–0.88) than for the other occurrences (MMF = 0.82–0.97, all combined). The values of KKNa (0.01–0.05) and MMF of preiswerkite are similar to those of "coexisting" paragonite and omphacite, respectively; amphibole in jadeitite has similar KKNa but lower values of MMF. Textures suggest that preiswerkite appears at the expense of paragonite. The Mg-rich composition indicates preiswerkite may be an intermediate or transitional phase to chlorite.

Phlogopite, which is found in a few jadeitites and omphacitites, generally has high Al^{VI} (0.9–1.3) and intermediate to high MMF (0.7–0.92). Phlogopite coexists with both phengite and paragonite (see Table 1) but not late-stage preiswerkite. Some phlogopite in omphacitites is replaced by chlorite (e.g. sample R-10). As suggested for preiswerkite, phlogopite indicates Mg + Fe enrichment and defines a discontinuous reaction boundary, although critical assemblages (e.g. Kfs–Ph–Phl–Qtz) for geothermobarometry are lacking.

Feldspar and similar minerals. All rock types contain virtually pure low albite (Table 5). Banalsite has a paracelsian-like structure that leads to 0.5 excess cations relative to the feldspar sum of 5 per 8 O (Table 5), and its composition resembles that in other jadeitites (Harlow & Olds, 1987). Cymrite is distinguished from celsian by its texture and oxide totals in probe analyses. If K-feldspar is not barian, it is near end-member composition. Barian K-feldspar, which often coexists with another Ba-rich phase, can exceed 0.25 Ba per 8 O and is thus hyalophane.

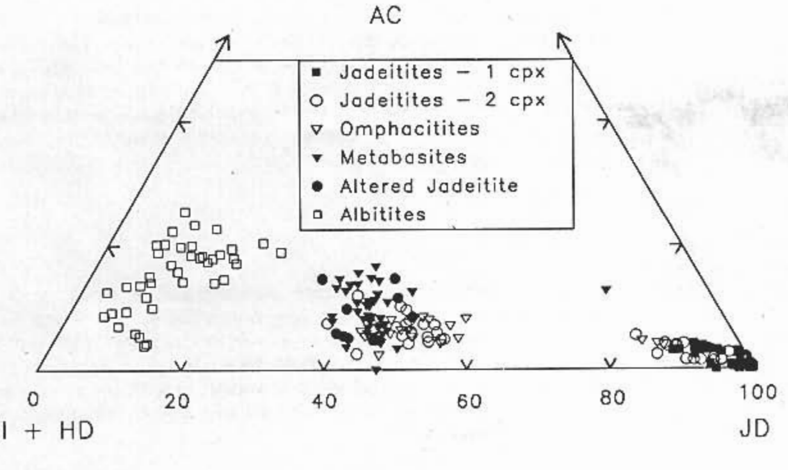

Fig. 6. Part of a ternary plot of pyroxene compositions in terms of the molar fractions of Di + Hd, Ac and Jd. Data are plotted for jadeitites. AMNH-33399, MVJ84-9D-1 and R-4 with only jadeitic Cpx; jadeitites AMNH-45049, R-1, R-12 and R-13 with both jadeite and omphacite; omphacitites NHMLAC-20368 and R-10; metabasites NHLMAC-20370 and MVJ84-51-1; an altered jadeitite/albitite MVJ84-12-1; and albitites MVJ84-25-1, MVJ84-60-1 and MVJ84-5C-1.

Table 5. Representative microprobe analyses of feldspars and feldspar-like minerals (8 O basis)

	1	2	3	4	5	6	7	8	9	10	11
SiO_2	67.82	68.36	37.38	69.09	64.56	67.70	31.34	68.59	63.81	54.64	32.64
TiO_2	0.00	0.00	0.08	0.00	0.01	0.00	0.17	0.00	0.01	0.03	0.17
Al_2O_3	19.10	20.40	32.12	19.36	18.30	19.39	25.96	19.78	18.31	20.87	27.27
Fe_2O_3	0.01	0.00	0.12	0.01	0.02	0.00	0.21	0.01	0.02	0.07	0.29
MgO	0.00	0.00	0.02	0.01	0.02	0.00	0.05	0.02	0.03	0.04	0.09
CaO	0.27	0.32	1.37	0.01	0.06	0.02	0.12	0.36	0.07	0.07	0.32
SrO	—	—	2.29	—	—	—	—	—	—	—	—
Na_2O	11.80	12.01	10.36	11.97	0.12	11.85	0.13	12.06	0.27	0.18	0.36
K_2O	0.01	0.01	0.02	0.03	16.56	0.04	0.20	0.02	15.81	12.17	0.33
BaO	0.02	0.00	17.06	0.02	0.12	0.07	37.03	0.05	0.74	11.19	38.00
Total	99.03	101.13	100.82	100.50	99.74	99.07	95.22	100.89	99.07	99.25	99.46
Si	3.00	2.96	1.98	3.00	3.00	2.99	2.02	2.98	2.99	2.75	2.01
Ti	0.000	0.000	0.003	0.000	0.000	0.000	0.008	0.000	0.000	0.001	0.008
Al	0.99	1.04	2.00	0.99	1.00	1.01	1.97	1.01	1.01	1.24	1.98
Fe^{3+}	0.001	0.000	0.005	0.000	0.001	0.000	0.010	0.000	0.001	0.003	0.013
Mg	0.000	0.000	0.001	0.001	0.001	0.000	0.005	0.001	0.002	0.003	0.008
Ca	0.013	0.015	0.077	0.001	0.003	0.001	0.009	0.017	0.003	0.004	0.021
Sr	—	—	0.070	—	—	—	—	—	—	—	—
Na	1.01	1.01	1.06	1.01	0.010	1.01	0.016	1.01	0.03	0.018	0.043
K	0.001	0.001	0.002	0.002	0.98	0.002	0.016	0.001	0.95	0.78	0.026
Ba	0.001	0.000	0.35	0.000	0.000	0.001	0.94	0.001	0.01	0.22	0.92
Total	5.01	5.02	5.55	5.01	5.00	5.01	4.99	5.02	4.99	5.02	5.02

(1) 'Primary' albite, MVJ84-9C-1, jadeitite; (2) secondary albite, MVJ84-9C-1, jadeitite; (3) banalsite, MVJ84-9C-1, jadeitite (nominally $NaBa_{0.5}Al_2Si_2O_8$); (4) secondary albite, MVJ90-24-2, jadeitite; (5) secondary K-feldspar, MVJ90-24-1, jadeitite; (6) albite, MVJ84-3-2, albite–mica rock; (7) cymrite, MVJ84-3-2, albite–mica rock (possible contamination in analysis); (8) albite, MVJ84-29-1, albite–mica rock; (9) K-feldspar, MVJ84-29-1, albite–mica rock; (10) hyalophane, MVJ84-29-1, albite–mica rock; (11) celsian, MVJ84-29-1, albite–mica rock.

Analcime, nepheline and cancrinite. Analyses for these minerals are given in Table 6. Analcime is consistently subsilicic, and (Na + K)/Al varies between 1.3 and 0.98 but is usually > 1.0. The lack of (Na + K) to Al balance is too large to ascribe to analytical error. An undetected cation or anion with low atomic number could explain the excess alkali. Natural analcime associated with sedimentary rocks and burial metamorphism varies substantially in Si content; low silica is sometimes associated with higher grade metamorphism (Coombs & Whetten, 1967). The subsilicic character of analcime in altered jadeitite may result from low a_{SiO_2} of the assemblages. KKNa of analysed analcime varies from 0.012 to 0.003 and always exceeds that of adjacent albite and precursor jadeite.

Nepheline is sodic (KKNa = *c.* 0.05–0.10) and slightly silicic, which is typical of metamorphic to metasomatic occurrences (e.g. Edgar, 1983). These compositions and the paragenesis via paragonite alteration contrast with the association of nepheline in jadeitite from Myanmar, Burma (Lacroix, 1930; Tilley, 1956). In the latter rocks, nepheline forms in veins at the expense of jadeite and has a composition near $Ne_{80}Ks_{20}$. The composition of comparably formed nepheline in sample R-12 is similar to that of nepheline in paragonite breakdown (Table 6).

Cancrinite in sample MVJ84-9D-1 contains insignificant S and Cl based on EDS spectra. The rare presence of cancrinite in jadeitite indicates locally high a_{CO_2} during alteration, which is consistent with a $CaCO_3$ presence in few jadeitites and albitites.

Amphibole. The blue pleochroic amphibole found in altered jadeitite is usually a magnesio-alumino-taramite with the approximate formula $Na_2CaMg_2FeFe^{3+}_{0.4}Al_{3.6}Si_6O_{22}(OH)_2$. In metamorphic or metasomatic rocks alumino-taramite has been reported only in altered eclogites from Norway (Smith, 1988) and France (Lasnier & Smith, 1989). The KKNa for Guatemalan amphiboles ranges from *c.* 0.025 to 0.05 and MMF from *c.* 0.5 to 0.64. Zoning occurs with respect to MMF; although patterns suggest a core-to-rim Mg enrichment, they are not uniform or regular. Amphibole from metabasites is similar in composition but richer in Fe and poorer in Al, tending toward pargasitic hornblende. In all of this amphibole, the A-site is fully occupied (Table 7).

In albitites lacking omphacite, all amphibole is tremolite/actinolite with MMF ranging from 0.75 to 0.90 and $Al^{IV} < 0.40$; in individual samples MMF varies by <0.1. Compositions of actinolite in actinolite–chlorite rock (analyses 8 & 9, Table 7) range from *c.* 0.85 to 0.93 in MMF.

Clinozoisite and zoisite. Whereas Fe content suggests clinozoisite predominates in jadeitites and altered jadeitites—$Fe_T/(Fe_T + Al)$ ranges from 0.10 to 0.21 (Table 8)—diffraction and optical data

Table 6. Representative microprobe analyses of analcime (96 O basis), nepheline (32 O basis) and cancrinite (Al + Si = 12 basis)

	1	2	3	4	5	6	7	8
SiO_2	49.36	52.02	51.53	43.28	42.76	43.09	43.97	36.21
TiO_2	0.00	0.0	0.04	0.00	0.01	0.00	0.00	0.00
Al_2O_3	24.60	24.36	25.47	34.69	34.88	35.74	34.84	32.80
FeO	0.00	0.00	0.00	0.05	0.03	0.00	0.02	0.00
MnO	0.00	—	0.00	0.00	0.01	0.02	0.01	0.14
MgO	0.00	0.04	0.00	0.01	0.00	0.00	0.02	0.00
CaO	0.02	0.05	0.04	0.94	0.63	0.58	0.51	5.85
Na_2O	15.42	15.08	15.29	19.51	17.80	17.89	18.35	19.56
K_2O	0.25	0.27	0.22	1.57	2.60	4.45	2.61	0.05
Total	89.65	91.83	92.59	100.06	98.72	101.76	100.32	94.61
Si	30.12	30.83	30.32	8.20	8.20	8.10	8.30	5.80
Ti	0.00	0.00	0.02	0.000	0.000	0.00	0.00	0.00
Al	17.69	17.01	17.67	7.75	7.89	7.92	7.75	6.20
Fe	0.00	0.00	0.00	0.008	0.004	0.000	0.003	0.00
Mn	0.00	—	0.00	0.000	0.002	0.004	0.001	0.019
Mg	0.00	0.04	0.00	0.002	0.000	0.000	0.005	0.00
Ca	0.02	0.04	0.02	0.19	0.13	0.12	0.10	1.01
Na	18.24	17.32	17.44	7.17	6.62	6.52	6.71	6.08
K	0.19	0.21	0.17	0.38	0.64	1.07	0.63	0.009
Total	66.25	65.43	65.63	23.70	23.48	23.73	23.50	19.11

(1) Analcime, R-15, jadeitite; (2) analcime, AMNH 33399, jadeitite; (3) analcime, MVJ84-9B-1, jadeitite; (4) nepheline ($Ne_{90}Ks_{4.8}Qtz_{2.8}$), MVJ84-9C-1, jadeitite, Pg replacement; (5) nepheline ($Ne_{83}Ks_{8.0}Qtz_{5.1}$), R-15, jadeitite, Pg replacement; (6) nepheline ($Ne_{82}Ks_{13}Qtz_{2.1}$), MVJ84-9B-1, jadeitite, Pg replacement; (7) nepheline ($Ne_{84}Ks_{7.8}Qtz_{5.4}$), R-12, jadeitite, Ab + Ne intergrowth; (8) cancrinite-like phase, MVJ84-9D-1, jadeitite, in vein.

Table 7. Representative microprobe analyses of amphiboles (23 O basis)

	1	2	3	4	5	6	7	8	9
SiO_2	42.92	42.79	41.04	40.79	40.04	40.84	56.75	56.01	56.89
TiO_2	0.30	0.46	0.04	0.32	0.32	0.72	0.09	0.10	0.02
Al_2O_3	19.81	19.79	20.65	14.36	17.48	17.99	2.15	1.94	0.54
Fe_2O_3*	0.31	0.00	2.73	0.67	2.25	0.00	0.00	0.00	0.00
FeO	10.55	12.08	11.50	17.75	19.23	17.76	4.19	7.30	4.33
MnO	0.41	0.45	0.53	0.31	0.13	0.48	0.16	0.19	0.20
MgO	9.95	8.40	7.99	7.28	4.56	5.95	21.31	19.04	22.04
Cao	7.86	7.41	7.51	9.90	7.84	7.45	10.36	10.55	12.65
Na_2O	6.12	5.93	6.07	4.37	4.99	4.62	2.62	1.50	0.80
K_2O	0.36	0.40	0.49	0.18	1.04	0.60	0.16	0.09	0.10
Total	98.59	97.70	98.54	95.94	97.89	96.41	97.78	96.73	97.58
Si	6.16	6.22	5.98	6.29	6.10	6.20	7.84	7.90	7.91
Al^{IV}	1.84	1.78	2.02	1.71	1.90	1.80	0.16	0.10	0.09
Ti	0.033	0.050	0.004	0.037	0.037	0.083	0.009	0.010	0.002
Al	1.51	1.61	1.52	0.90	1.24	1.42	0.19	0.22	0.000
Fe^{3+}*	0.033	0.000	0.30	0.078	0.26	0.000	0.00	0.000	0.000
Fe^{2+}	1.27	1.47	1.40	2.29	2.45	2.25	0.48	0.86	0.50
Mn	0.050	0.055	0.065	0.040	0.017	0.062	0.019	0.023	0.023
Mg	2.13	1.82	1.74	1.68	1.04	1.35	4.39	4.00	4.57
Sum C†	5.02	5.01	5.03	5.02	5.04	5.16	5.08	5.12	5.10
Ca	1.21	1.16	1.17	1.64	1.28	1.21	1.53	1.59	1.88
Na_B	0.77	0.84	0.80	0.34	0.68	0.63	0.38	0.29	0.02
Sum B	2.00	2.00	2.00	2.00	2.00	2.00	2.00	2.00	2.00
Na_A	0.93	0.83	0.91	0.96	0.80	0.73	0.32	0.13	0.20
K	0.066	0.074	0.090	0.036	0.20	0.12	0.027	0.016	0.018
Total	16.00	15.91	16.00	16.00	16.00	15.85	15.35	15.14	15.22

(1) Magnesio-alumino-taramite, more magnesian, MVJ84-9C-1, jadeitite; (2) magnesio-alumino-taramite, more ferroan, MVJ84-9C-1, jadeitite; (3) magnesio-alumino-taramite, MVJ84-9B, jadeitite; (4) ferroan pargasite, NHMLAC 20370, metabasite; (5) ferroan taramite, MVJ84-51-1, metabasite; (6) ferroan taramite, MVJ84-12-1, highly altered jadeitite; (7) tremolite, MVJ84-57-1, tremolite/actinolite schist; (8) actinolite, MVJ84-57-1, albitite; (9) actinolite, MVJ84-66-1, chlorite–actinolite rock.

* Fe^{3+} calculated to reduce cation total to 16.0.

† Cations in Sum C (M_{1-3}) in excess of 5.0 are added to B(M_4) cations.

indicate the presence of zoisite. Analyses of zoisite from albitites show total Fe as $Fe_2O_3 < 2.0$ wt%, and from 0.5 to 2.5 wt% SrO; Fe and Sr are enriched in the rims of crystals. Weak pleochroism and a few probe analyses indicate compositions transitional between clinozoisite and epidote, i.e. 1 Fe^{3+} per 25 O, in metabasites. Some clinozoisite in metabasites contains > 10 wt% SrO (analysis 4, Table 8).

Chlorite grains in actinolite–chlorite rock are sheridanite/clinochlore (nomenclature after Hey, 1954) with MMF of 0.82–0.89 (Table 8) and are less homogeneous than coexisting actinolite. Clinochlore in omphacitite ranges from 0.85 to 0.92 in MMF values of 0.90–0.96. Some chlorite grains are "intergrown" with phengite in the albite–mica rocks.

DISCUSSION

Tectonic inclusions and zoning pattern

Jadeitites from Guatemala, like others known, occur as tectonic inclusions in a serpentinite–matrix melange. The field and petrographical relations reveal a core primarily of jadeitite, infiltrated and surrounded by increasing amounts of albitite, a boundary blackwall zone of chlorite ± actinolite and finally the serpentinite matrix (see Fig. 2). Some blocks consist only of jadeitite alteration products. Since albitite and albite mica rock are found together in the field, they may have formed in a single event. Metabasites are found with jadeitites, and the veins of jadeitite in metabasite indicate that metabasite predates or is coeval with jadeitite. However, the spatial relationship of metabasites to jadeitites and albitites is unclear.

Primary jadeitite and the question of jadeitite protoliths

The near monomineralic constitution of jadeitites and their restricted provenance indicates they are metasomatic rocks (Coleman, 1961, 1980). Other jadeitite occurrences sometimes manifest a concentric zoning pattern with a non-jadeitite core that typically suggests an albititic protolith (e.g. Chhibber, 1934; Chihara, 1971), but no evidence of a protolith was found in this study. If Guatemalan jadeitites were created by replacement, the protolith texture or mineralogy cannot be recognized, except perhaps for muscovite inclusions in jadeite grains and corroded titanites in jadeitites. Moreover, the advanced alteration of jadeitite to albitite obscures prealteration textures and mineralogy. None the less, it is useful to examine the potential reactions that can form jadeitite.

Primarily jadeitite consists of jadeite, white mica, and probably albite ± titanite, apatite, zircon and possibly (clino)zoisite (Tables 1 & 2). Without quartz, jadeitite cannot be formed isochemically from a reaction like

$$\underset{\text{Albite}}{NaAlSi_3O_8} \Rightarrow \underset{\text{Jadeite}}{NaAlSi_2O_6} + \underset{\text{Quartz}}{SiO_2} \quad (1)$$

However, the isochemical reaction

$$\underset{\text{Albite}}{NaAlSi_3O_8} + \underset{\text{Nepheline}}{NaAlSiO_4} \Rightarrow \underset{\text{Jadeite}}{NaAlSi_2O_6} \quad (2)$$

is also inappropriate, because syenitic (silica-depleted) rocks are unknown in the region.

The serpentinite host is thought to facilitate the formation of jadeitite (e.g. Coleman, 1961, 1980; Dobretsov, 1963, 1984). For a serpentinizing or serpentinized ultramafic rock, fluid-enhanced interactions with a tectonic block could be signficant for many chemical species. Silica activity will be strongly affected by the olivine-to-pyroxene ratio of the original ultramafic rock in the serpentinite-forming reactions

$$\underset{\text{Olivine}}{Mg_2SiO_4} + \underset{\text{Pyroxene}}{MgSiO_3} + \underset{\text{W}}{2H_2O} \Rightarrow \underset{\text{Serpentine}}{Mg_3Si_2O_5(OH)_4} \quad (3)$$

and, more importantly,

$$\underset{\text{Olivine}}{2Mg_2SiO_4} + \underset{\text{W}}{3H_2O} \Rightarrow \underset{\text{Serpentine}}{Mg_3Si_2O_5(OH)_4} + \underset{\text{Brucite}}{Mg(OH)_2}. \quad (4)$$

Silica activity should be reduced below unity by serpentinization of a dunitic to harzburgitic protolith. Unsheared serpentinites indicate such protoliths along the Motagua Fault (Bertrand & Vuagnat, 1975, 1976, 1977, 1980).

Table 8. Representative microprobe analyses of zoisite, clinozoisite (25 O basis) and chlorite (28 O basis).

	1	2	3	4	5	6	7	8	9	10	11
SiO_2	38.94	37.70	38.27	35.48	38.82	35.66	35.86	32.83	32.45	39.69	38.20
TiO_2	0.06	0.08	0.18	0.09	0.10	0.03	0.03	0.01	0.08	0.02	0.01
Cr_2O_3	—	—	0.02	—	—	0.08	0.03	—	—	—	0.11
Al_2O_3	28.51	25.42	25.84	21.93	31.31	13.71	14.96	15.09	16.2	12.48	17.50
Fe_2O_3*	5.23	9.93	9.49	11.03	0.98						
FeO						4.90	6.77	6.85	9.39	5.42	2.20
MnO*	0.04	0.06	—	0.07	0.04	0.09	—	0.04	0.07	0.05	—
MgO	0.03	0.02	0.31	0.10	0.04	32.57	30.18	31.70	27.91	29.02	28.49
CaO	23.98	23.57	22.68	15.57	23.39	0.17	0.23	0.06	0.11	0.63	0.40
SrO	0.05	0.00	—	10.27	1.36	—	—	—	—	—	—
Na_2O	0.07	0.02	0.00	0.02	0.00	0.00	0.05	0.00	0.95	0.05	0.00
K_2O	—	—	0.01	—	—	0.05	0.17	0.01	0.17	0.15	0.15
Total	96.90	96.80	96.80	94.57	96.04	87.26	88.28	86.59	87.36	87.51	87.05
Si	6.07	6.00	6.05	6.10	6.06	6.72	6.73	6.32	6.29	7.40	7.02
Al^{IV}						1.28	1.28	1.68	1.71	0.60	0.98
Ti	0.007	0.009	0.022	0.013	0.011	0.004	0.009	0.001	0.012	0.002	0.002
Cr	—	—	—	—	—	0.012	0.004	—	—	—	0.016
Al	5.25	4.77	4.82	4.46	5.76	1.76	2.03	1.74	2.00	2.14	2.81
Fe^{3+}*	0.61	1.19	1.13	1.43	0.12						
Fe^{2+}*						0.77	1.06	1.10	1.52	0.85	0.34
Mn*	0.005	0.008	—	0.010	0.005	0.014	—	0.007	0.011	0.001	—
Mg	0.008	0.004	0.072	0.025	0.009	9.15	8.44	9.10	8.07	8.07	7.81
Ca	4.01	4.02	3.84	2.90	3.91	0.035	0.046	0.013	0.022	0.13	0.078
Sr	0.004	0.000	—	1.03	0.12	—	—	—	—	—	—
Na	0.021	0.008	0.000	0.008	0.000	0.000	0.019	0.000	0.36	0.018	0.001
K	—	—	0.002	—	—	0.013	0.041	0.001	0.042	0.035	0.035
Total	15.99	16.01	15.94	15.94	15.99	19.76	19.65	19.97	20.04	19.25	19.09

(1) Clinozoisite, MVJ84-9C-1, jadeitite; (2) clinozoisite, MVJ84-9C-1, jadeitite; (3) epidote, MVJ84-23-1, metabasite (includes 0.14 wt% BaO); (4) strontian clinozoisite, MVJ87-14-1, metabasite; (5) zoisite, MVJ84-29-1, albite–mica rock; (6) clinochlore, MVJ84-41-4, omphacitite; (7) clinochlore, R-10, omphacitite; (8) clinochlore/sheridanite, MVJ84-66-1, chlorite–actinolite rock; (9) clinochlore/sheridanite, MVJ87-1-2, chlorite–actinolite rock; (10) penninite, MVJ84-24-2, albitite; (11) clinochlore, MVJ84-23-2, albite–mica rock.

* For (clino)zoisites only, all Fe and Mn calculated as trivalent.

Thus, reaction (1) may not be univariant, because an a_{SiO_2} of <1 could be imposed by reactions in the serpentinite. A revised reaction is

$$\underset{\text{Albite}}{NaAlSi_3O_8} \Rightarrow \underset{\text{Jadeite}}{NaAlSi_2O_6} + SiO_2^{aq}, \qquad (1A)$$

in which the interaction of an aqueous fluid between serpentinite and jadeitite is critical.

The mineralogy of jadeitites requires (1) a protolith of essentially jadeite composition, (2) Na-metasomatism of a protolith with high $Al/(Fe_T + Mg)$ (or interaction with fluids having high Na activity compared to K, Ca, etc.) or (3) a fractionation process that extracts jadeitite components from some protolith and crystallizes them as bodies within the serpentinite. For a metasomatic process in which alkalis and silicas are the most significant mobile species, an aluminous rock could be an appropriate jadeitite protolith.

Candidates for protoliths are limited. McBirney (1963) noted inclusions of felsic and mafic pelitic schist, amphibolite and marble of the adjacent Chuacús Formation in serpentinites about 70 km west of the jadeitite occurrence. He also described amphibolite inclusions consisting of albite and uralitized jadeite; no data are available for these minerals and rocks. In the study area, the felsic rocks in fault contact with serpentinite are the San Agustín gneiss and the Jones metasedimentary rocks. The San Agustín gneiss is a metagranitoid composed of K-feldspar, quartz, muscovite, albite, biotite, epidote and garnet (Bosc, 1971). The Jones metasedimentary rocks (Newcomb, 1975) and undivided Chuacús schists (McBirney, 1963; Bosc, 1971) contain a higher proportion of quartz and mica than feldspar compared to the San Agustín gneiss. Mafic parts of these schists contain abundant titanite, which might explain the origin of corroded titanite in some jadeitites.

Plagiogranite, a typical component of ophiolite suites, is a hypothetical protolith, particularly since Coleman (1961) suggested that quartz keratophyres (plagiogranite-like rocks) were metasomatized and remobilized to form the jadeitite in the New Idria serpentinite body of California. However, no plagiogranite is known from the ophiolite-like terrane along the Motagua Fault Zone; plagiogranite is not a likely protolith.

Reaction paths between potential protoliths and jadeitites can be estimated by examining pairs of bulk compositions. Some patterns are evident from the concentration ratios (jadeitite-to-protolith) of major element oxides (Table 9) for representative rock compositions. Relative increases are uniformly required for Na_2O, 22–18 times, and Al_2O_3, 1.1–2.5 times; relative decreases are required for K_2O, 0.004–0.15 (to 2.2 relative to a plagiogranite) times, for FeO, 0.03–0.72 times and generally for SiO_2, 0.7–1.2. The chemical changes are primarily (1) an exchange of Na for K, (2) an exchange of Na couples like NaAl for CaMg and (3) a reduction of silica. Silica decrease may be explained by low a_{SiO_2} in serpentinite (Coleman, 1961, 1980; Dobretsov, 1984). The

Table 9. Comparison of possible protolith to jadeitite and albitite compositions.

	Jadeite	Concentration ratios (Jadeitite/protolith)						Albitite/jadeitite
	TD-1	OM-32	SAG	DN-1	DN-5	DN-21	DN-22	18
SiO_2	61.8	0.85	0.88	0.79	1.03	0.94	1.17	1.11
TiO_2	0.02	0.04	0.05	0.02	0.03	0.02	0.02	0.50
Al_2O_3	22.39	1.67	1.51	2.34	1.27	1.23	1.29	0.76
Fe_2O_3	0.15	0.05	0.10	0.12	0.05	0.03	0.04	1.80
FeO	0.30	0.33	0.16	0.15	0.08	0.41	0.07	1.87
MgO	1.68	1.68	1.49	1.71	0.60	0.60	0.50	0.21
CaO	0.60	0.20	0.28	0.38	0.14	2.14	0.10	1.67
Na_2O	12.43	2.35	4.67	5.98	3.49	7.44	15.7	0.86
K_2O	0.26	2.17	0.06	0.15	0.15	0.08	0.05	0.50
	ZCS-20							L
SiO_2	57.08	0.78	0.81	0.73	0.95	0.87	1.08	1.16
TiO_2	0.25	0.53	0.63	0.25	0.38	0.24	0.27	0.76
Al_2O_3	19.30	1.44	1.30	2.01	1.10	1.06	1.12	0.67
Fe_2O_3	6.06	2.16	4.21	4.66	1.95	1.15	1.55	0.14
FeO	0.53	0.58	0.29	0.27	0.17	0.72	0.12	1.51
MgO	1.66	1.66	1.47	1.69	0.60	0.59	0.49	3.86
CaO	3.08	1.03	1.42	1.95	0.71	11.0	0.53	1.32
Na_2O	11.73	2.21	4.41	5.64	3.29	7.02	14.8	0.57
K_2O	0.21	1.75	0.05	0.13	0.12	0.06	0.04	1.17
	Pa–Jd							18
SiO_2	58.7	0.91	0.83	0.75	0.98	0.90	1.11	1.16
TiO_2	0.41	0.45	1.02	0.41	0.63	0.40	0.44	0.025
Al_2O_3	24.2	1.61	1.64	2.53	1.38	1.33	1.40	0.71
Fe_2O_3	0.53	0.16	0.37	0.41	0.17	0.10	0.14	0.51
FeO	0.13	0.03	0.07	0.07	0.03	0.18	0.03	4.3
MgO	0.43	0.13	0.38	0.44	0.15	0.15	0.13	0.81
CaO	1.00	0.18	0.46	0.63	0.23	3.57	0.17	1.00
Na_2O	14.37	3.69	5.40	6.91	4.04	8.60	18.2	0.74
K_2O	0.02	0.11	0.005	0.01	0.01	0.006	0.004	6.5

Sources of bulk composition are as follows: jadeitite (McBirney *et al.*, 1967; Silva, 1970; and modal estimates from this study), plagiogranites (Coleman & Donato, 1979), albitites (Bertrand & Vuagnat, 1976; Silva, 1970; Donnelly & Newcomb, unpubl. data), Jones metasediments and Chuacús granitic gneisses (Donnelly & Newcomb, unpubl. data).

TD-1, jadeitite (Silva, 1970); OM-32, plagiogranite (Coleman & Donato, 1976); SAG, average of 26 San Agustín granites (Donnelly & Newcomb, unpubl. data); DN-1, migmatite (ibid); DN-5, Jones metasediment (ibid); DN-21, Jones mica schist (ibid); DN-22, Jones mica schist (ibid); ZCS-20, jadeitite (Silva, 1970); Pa-Jd, paragonite-bearing jadeitite, consisting of 92% Jd, 5% Pa, 2% Ab, 1% Ttn, by weight, calculated from mineral compositions; 18 and L, albitites (ibid).

Na_2O increase indicates that the fluid involved must have had a high a_{Na} and exchange potential (sufficient water-to-rock ratio). The Al_2O_3 increase suggests that it is immobile or that an NaAl couple, in solution, replaced other cations to produce $Na/Al \approx 1$. The Mzl rocks are slightly richer in K and Mg versus Na and (Mg + Fe) than the RLP jadeitites.

Many of the Guatemala jadeitites are composed of or heavily infiltrated by jadeitite vein material in fractures. Thus, jadeitites and/or their protoliths may have undergone pressure solution – fracture redeposition such that jadeitites are largely reworked vein material. For such a situation, solution and recrystallization by a fluid saturated with respect to jadeitite phases is more applicable than complete metasomatism of a protolith. If the process is dominant, jadeitite protoliths may never be found. However, a source for the jadeitite chemical components is still needed; pelitic or felsic rocks are obvious candidates.

A dissolution/precipitation mechanism begs examination of the solubility of the jadeitite and protolith minerals as a function of P/T, fluid composition and fluid flow. Some experimental results show increasing solubility of silica with respect to alkali aluminosilicates with increasing pressure P (e.g. Woodland & Walther, 1987), thus favouring silica depletion by dissolution in a fluid-flushed environment. However, in high-P/T metasomatism in the Tauern window, Na decreases along with Si (Selverstone *et al.*, 1991). Calculations by Dipple & Ferry (1990) and Ferry & Dipple (1991) show the effects of $P-T$ gradients on exchange of Si, K, Na, Ca and Mg between rock and fluid flowing up a vertical fault. If fluid flows down a temperature gradient to lower pressure conditions, it becomes saturated in SiO_2, but not Na or K. If upward flow occurs in an inverted temperature gradient, soda and silica saturations can occur together. However, the initial a_{Na} must be relatively high, which suggests a seawater-like fluid source.

Fluid flow and the tectonic environment of a serpentinite–matrix melange probably work together to form jadeitite. The serpentinite host provides a silica sink and a weak boundary for concentration of fault movement. The conduit provided by the Motagua Fault Zone provides a mechanism for sequential fracture filling. Pulsed fractures permit entrance of fresh fluid into opened cavities; each pulse of fluid could yield a rhythmic band on zoned pyroxene crystals in veins, as has also been interpreted for zoned omphacite in veined Alpine eclogites by Philippot & Selverstone (1991).

Jadeitite alteration and formation of albitite

Several reactions are required in jadeitite alteration. Many of these are net transfer reactions which are given here in a simplified chemical system with end-member phase compositions. The first reaction is the hydration of jadeite to produce the analcime observed in fractures and on grain boundaries:

$$\underset{\text{Jadeite}}{NaAlSi_2O_6} + \underset{\text{W}}{H_2O} \Rightarrow \underset{\text{Analcime}}{NaAlSi_2O_6 \cdot H_2O}. \qquad (5)$$

One sample (R-12) demonstrates the reaction Jd $\Rightarrow$ Ne + Ab (the reverse of reaction 2), followed by analcime. The texture indicates either

$$\underset{\text{Nepheline}}{NaAlSiO_4} + \underset{\text{Albite}}{NaAlSi_3O_8} + \underset{\text{W}}{H_2O} \Rightarrow \underset{\text{Analcime}}{2NaAlSi_2O_6 \cdot H_2O}. \qquad (6)$$

or

$$\underset{\text{Nepheline}}{NaAlSiO_4} + SiO_2^{aq} + \underset{\text{W}}{H_2O} \Rightarrow \underset{\text{Analcime}}{NaAlSi_2O_6 \cdot H_2O}, \qquad (7)$$

and presents an essentially invariant or univariant assemblage depending primarily upon whether $P_{H_2O} = P_T$ (see below). The alteration textures indicate replacement of analcime by albite:

$$\underset{\text{Analcime}}{NaAlSi_2O_6 \cdot H_2O} + SiO_2^{aq} \Rightarrow \underset{\text{Albite}}{NaAlSi_3O_8} + \underset{\text{W}}{H_2O} \qquad (8)$$

In some cases, however, albite evidently replaced jadeite by the reverse of reaction (1A). As the jadeite component is consumed, the relict pyroxene becomes increasingly diopsidic (augitic), explaining the blebs of augite in albitites.

The other major breakdown product of jadeitic pyroxene is magnesio-taramitic amphibole which probably sequesters augite and acmite components of the original pyroxene. The values of $Na/(Al + Fe^{3+})$ in pyroxene and amphibole are *c.* 1, whereas $Ca/(Mg + Fe)$ decreases from 1 to ≤ 0.5, respectively. This suggests that amphibole formation requires interaction with chlorite or serpentinite via the fluid. With increasing albitization, the amphibole changes to actinolite, with no observed intermediate compositions. This change probably reflects a transition from jadeite-stable to albite + chlorite-stable assemblages, as discussed below.

Remarkable reactions are recorded in the breakdown textures of paragonite. The most frequently observed rims around paragonite consist of sodic nepheline, which suggests

$$\underset{\text{Paragonite}}{NaAl_3Si_3O_{10}(OH)_2} + 2Na^+ \Rightarrow \underset{\text{Nepheline}}{3NaAlSiO_4} + 2H^+, \quad (9)$$

and another rimming phase is banalsite, which suggests a reaction like

$$\underset{\text{Paragonite}}{4NaAl_3Si_3O_{10}(OH)_2} + 2Na^+ + 3Ba^{2+} \Rightarrow \underset{\text{Banalsite}}{3BaNa_2Al_4Si_4O_{16}} + 8H^+. \quad (10)$$

Both reactions indicate the influence of the fluid on the stability and composition of the solid phases.

Clinozoisite is closely associated with paragonite and perhaps phengite breakdown. It is a further example of initial reactions that preserve Al/Si but exchange large cations. A suggested reaction is

$$\underset{\text{Paragonite}}{NaAl_3Si_3O_{10}(OH)_2} + 2Ca^{2+} + \underset{\text{W}}{H_2O} \Rightarrow \underset{\text{Clinozoisite}}{Ca_2Al_3Si_3O_{12}(OH)} + Na^+ + 3H^+. \quad (11)$$

The formation of preiswerkite is texturally and compositionally related to paragonite much as taramite is to pyroxene; the value of Na/Al between the former two phases is roughly constant but the content of $(Mg + Fe^{2+})$ increases in the alteration phase. Thus, preiswerkite also indicates the addition of a mafic component from the serpentinite through the fluid. Nepheline disappears by reactions (7) plus (8). It is, at most, locally stable during alteration and is unstable in the albitite phase assemblage.

Albitite compositions are compared to jadeitite as major element concentration ratios between two albitites (Silva, 1970) and jadeitites (Table 9). The results are generally consistent with the interpretations of alteration reactions, in particular requiring SiO_2 increase. However, MgO ratios vary, which may indicate inappropriate pairing of rock compositions.

Textures of jadeite grains: alteration or relict protolith

There are several interpretations for the abundant mineral inclusions in cores of jadeite grains in many jadeitites. First, jadeite may be similar to garnet in its propensity to include other phases as grains grow, preserving successive metasomatic assemblages. Second, if jadeite grew by replacement, the inclusions may represent protolith mineralogy. Third, inclusions may be alteration minerals. Finally, if rhythmic zoning of jadeite records pulses of changing conditions, inclusions may represent oscillating conditions of growth, alteration and further growth.

Many inclusions are elongated along the *c*-axis of jadeite, the direction of greatest diffusivity (e.g. Farver, 1989), the intersection of jadeite cleavage, and an avenue of subgrain-boundary diffusion. In order of decreasing abundance, the inclusions are albite, white mica, amphibole, zoisite, preiswerkite and analcime. Albite inclusions are uninformative. Except for rare muscovite inclusions, the white mica inclusions are identical to micas intergrown with jadeite and thus probably are simple coeval growth inclusions. Amphibole, analcime, zoisite and preiswerkite are clearly alteration products. Only muscovite inclusions suggest affinity with a protolith. The paragenetic affinity of inclusions suggest a complex history for jadeitites that involved changes in conditions such that jadeite (and white mica) first grew, then albite, more jadeite, then alteration-like minerals formed, then jadeite overgrowth, and finally alteration conditions dominated.

Physical conditions of petrogenesis

A petrogenetic grid for P–T reaction equilibria was calculated with the program GE0-CALC (Berman *et al.*, 1987) using the data of Berman (1988) unless otherwise noted. Thermodynamic data for nepheline (Berman, pers. comm.) and analcime (see Appendix) were included.

Jadeitites

The simplest system that approximates the phase relations of jadeitites ($Jd + Pg/Ph + Ab \pm Omp \pm Ttn$) is $NaAlSiO_4$–SiO_2–H_2O (NASH; Liou, 1971). The presence of jadeite, albite and aqueous fluid (e.g. H_2O-rich fluid inclusions in jadeite and vein textures) and the lack of primary analcime or quartz constrain pressures below the $Jd + Qtz = Ab$ reaction (1) and above the $Jd + W = Anl$ reaction (5). The experimental calibration of reaction (5) is critical to interpretations of jadeitite petrogenesis. The experiments of Manghnani (1970), where $P_{H_2O} = P_T$ (see Fig. 7a), are most consistent with other calibrations (e.g. Kim & Burley, 1971). The invariant for reactions (1), (5) and $Anl + Qtz = Ab + W$ (Liou, 1971; Thompson, 1971) extrapolates to $<100°$ C and does not plot with the chosen analcime data in GE0-CALC except at very low a_{SiO_2} (Fig. 7b). Silica solubility in analcime was not modelled, but it is probably important in natural analcime (e.g. Helgeson *et al.*, 1978). At 100° C the pressure range for jadeitite

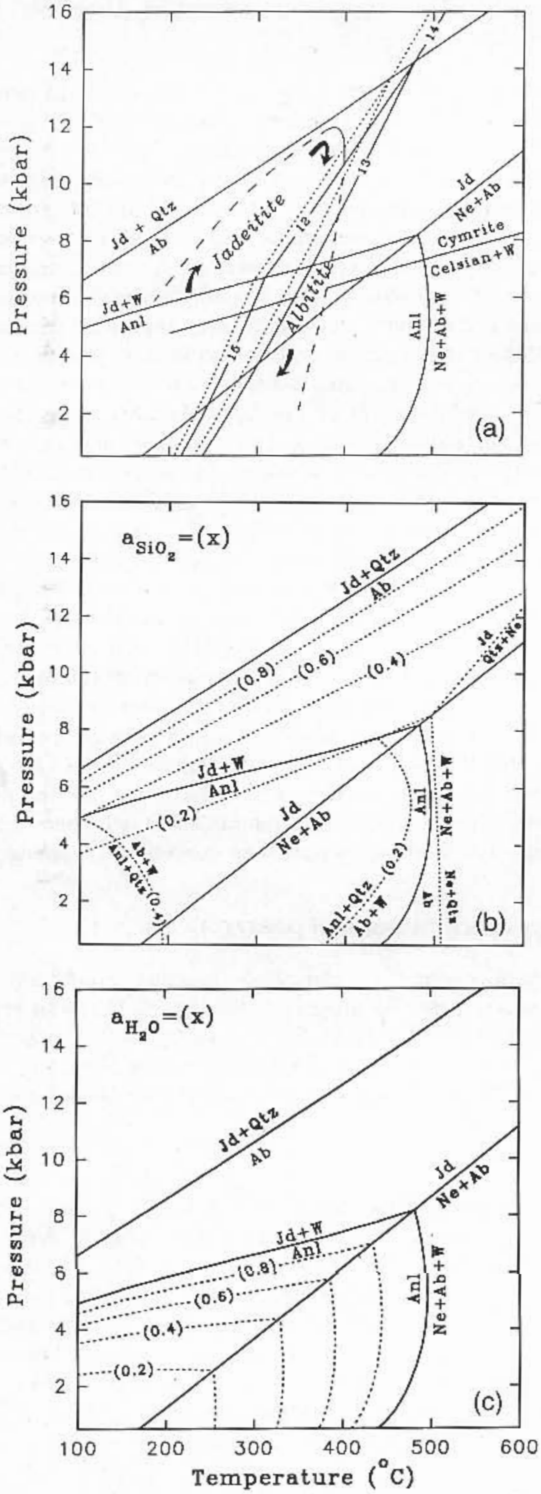

Fig. 7. *P–T* diagrams for critical discontinuous reactions relevant to Guatemalan jadeitite and albitite petrogenesis. Stable reactions are shown as solid lines; dashed lines represent reactions at reduced cZo, Pg, H_2O or SiO_2 activity. (a) General constraints at unit activities; reactions defined by an integer include (12) 4 Lw + 2 Jd = Ab + Pa + 2 cZo + 6 W, (13) 4 Lw + Ab = 2 Qtz + Pa + 2 cZo + 6 W, (14) 4 Lw + Jd = Qtz + Pa + 2 cZo + 6 W and (15) 4 Lw + 2 Anl = Ab + Pa + 2 cZo + 8 W (dashed lines represent $a_{cZo} = 0.69$ and $a_{Pg} = 0.95$, taking into account compositions of cZo and Pg in typical jadeitites). A suggested outer envelope for conditions of formation of jadeitite and jadeitite alteration and albitite is defined by curved coarsely dashed line. (b) Stable portion of NASH system contoured for a_{SiO_2} from 1.0 to 0.2. (c) Stable portion of NASH system contoured for a_{H_2O} from 1.0 to 0.2.

stability is from 5 to 6.5 kbar. Maximum temperature is limited by the almost vertical bulk melting curve for the system at *c.* 600° C (e.g. Thompson & Thompson, 1976) and the reaction Jd = Ne + Ab (2), which limits pressure to between 11 and 17 kbar (Fig. 7a).

These estimates represent all phases at unit activity. The absence of quartz requires $a_{SiO_2} < 1$; calculated contours of a_{SiO_2} in Fig. 7(b) indicate that its value could range from 0.2 to *c.* 1 (*c.* $0.7 \leq \log a_{SiO_2} < 0$) and maintain jadeite stability above the Jd + W = Anl reaction (5). As $a_{H_2O} < 1$, minimum pressure from reaction (5) must be somewhat lower. The presence and saline composition (*c.* 7% NaCl) of fluid inclusions in Jd (Harlow, 1986) indicates a substantial a_{H_2O}. An a_{H_2O} of 0.8 lowers pressure by only *c.* 0.5 kbar for reaction (5) (Fig. 7c). Thus, Guatemalan quartz-free jadeitites evidently represent high-*P–T* parageneses.

Celadonite-rich muscovite is associated with conditions of relatively high pressure. Jadeitites lack the limiting assemblage of Ph–Phl–Kfs–Qtz, but, the calibration of Massonne & Schreyer (1987) yields a minimum pressure estimate for the assemblage Jd–Ph–Phl–Kfs(?) of three jadeitites (Table 1). Phengite in these samples has Si contents of 3.24–3.36 (per 11 O) which yields 3.5–7 kbar at 300° C or 6.8–10.3 kbar at 500° C.

The presence of clinozoisite and absence of lawsonite in jadeitites permit the application of an important limiting reaction:

$$\underset{\text{Lawsonite}}{4CaAl_2Si_2O_7(OH)_2{\cdot}H_2O} + \underset{\text{Jadeite}}{2NaAlSi_2O_6} \Rightarrow \underset{\text{Clinozoisite}}{2Ca_2Al_3Si_3O_{12}(OH)_2} + \underset{\text{Paragonite}}{NaAl_3Si_3O_{10}(OH)_2} + \underset{\text{Albite}}{NaAlSi_3O_8} + \underset{\text{W}}{6H_2O}. \quad (12)$$

However, (clino)zoisite may not be an equilibrium phase in many jadeitites. The experimentally observed reaction 4 Lw + Ab = 2 Qtz + Pa + 2 Czo + 6 W (13) of Heinrich & Althaus (1980) is essentially identical to the calculated reaction (Fig. 7a). The intersection of reactions (5) and (12), adjusted for compositions of clinozoisite and paragonite in jadeitite, defines a minimum temperature of *c.* 300° C at $a_{H_2O} = 1$ for (clino)zoisite-bearing jadeitites (Fig. 7a). Clinozoisite textures suggest that this constraint applies to the end of jadeitite formation or to the onset of albitization.

The evidence of the Jd–Omp–Augite solvus in jadeitite pyroxenes indicates $T < 400°$ C, but the solvus is not sufficiently well constrained to interpret the gap between jadeite and omphacite compositions (Carpenter & Smith, 1981). The microstructures in typical omphacite in Motagua jadeitite were examined by Carpenter (1979, 1981), who found abundant anti-phase domains (APDs) *c.* 100–200 Å in size. Based on T–P estimates of 350–400° C and 6–8 kbar, which relied on misinformation that lawsonite was present, Carpenter (1981) estimated that the microstructures required *c.* 10^5 years to form. Following his analysis (Carpenter, 1981), higher temperature estimates yield unrealistically short periods for microstructure growth (e.g. 10^{-2} years at 600° C); at 450° C the growth time is only 100 years. If the T–T–T curves are correct, then maximum temperature for omphacite-bearing assemblages is 300–400° C. In conclusion, primary jadeitite could have formed at a range of pressures (see Fig. 7) with maximum $T = c.$ 400° C.

Alteration of jadeite

Analcime replacement of jadeite places P–T conditions below the Anl = Jd + W reaction (5) (see Fig. 7). If $P_{H_2O} < P_T$, the reaction pressure is lowered as shown by the a_{H_2O} isopleths in Fig. 7(c). Such a reduction in a_{H_2O} ($0.6 > a_{H_2O} \geq 0.4$) explains the breakdown Jd ⇒ Ne + Ab observed in sample R-12 at $T < 400$° C, but reduced a_{H_2O} was evidently local and rare. Because reaction (5) is indicated by most textures, its slope is very shallow, silica is not involved in it, and because of the abundant evidence for the presence of an aqueous fluid during alteration, the P–T trajectory for jadeitite alteration most likely was dominated by decreasing pressure.

The presence of relatively pure late-stage K-feldspar in jadeitites and albitites provides an estimate of equilibration temperature, although the phase composition could easily represent an annealing condition on cooling. From various strain-free albite–K-feldspar solvi (e.g. in Yund & Tullis, 1983) the values of Or_{96-98} indicate $T < 300$° C, up to $P = 10$ kbar.

Albite-rich rocks

Albitites contain Ab + Tr + Cpx ± Qtz ± Zoi ± Chl ± Ph. Because the albitites form by alteration of jadeitite, the interpretation of decreased pressure for jadeitite alteration, discussed above, indicates that these rocks formed at $P < c.$ 7.5 kbar (at 400° C). Albitites with Ab + Qtz + Zoi + Tr + Chl define a greenschist facies assemblage in the metabasite petrogenetic grid of Liou *et al.* (1985) at 350–400 °C, 3–8.5 kbar.

The albite–mica rock assemblage Ab + Ph + Zoi + Chl ± Qtz ± Mc ± Cel/Cym falls within a large region of the greenschist and amphibolite facies limited by reaction (1), the paragonite stability field and the reactions Kln + Kfs = Ab + Ms + Qtz + H_2O and probably Lw + Ab = Pg + Zoi + Qtz + W (Thompson & Thompson, 1976). In albite–mica rocks containing Ph + Chl + Kfs ± Phl, Si cations in phengite range from 3.35 to 3.45 which yield minimum pressures of 7–9 kbar at 300° C or 8–10 kbar at 400° C (Massonne & Schreyer, 1987). Phengite from cymrite-bearing sample MVJ84-3-2 has an Si content > 3.45. The presence of celsian (versus cymrite) in albite–mica rocks requires $P < c.$ 6.5 kbar at 400° C and $P_{H_2O} = P_T$ (Fig. 7a), based on the calibration of Cym = Cel + W by Graham *et al.* (1992). Discrepancies between the phengite and cymrite/celsian barometry may reflect late-stage Ba enrichment. Albite–mica rocks show a pressure-dependent trajectory that extends from higher-P jadeitite stability conditions to lower-P alteration conditions. Thus, albitites formed at lower pressure at the expense of jadeitite; some albite–mica rocks could have formed at pressures comparable to jadeitite (but at higher a_{SiO_2}) and yet others at lower pressure conditions. Both albite-rich rock types require temperatures of 300–400° C to stabilize zoisite, which puts them at the high end of the jadeitite temperature spectrum (Fig. 7).

Further comments on chemical conditions

Jadeitites and albitites have been strongly influenced by changing a_{SiO_2}. Contouring of a_{SiO_2} in Fig. 7(b) for reaction (1) indicates the jadeitite mineral suite (and the fluid that affected it) can be constrained to $c.\ -0.7 \leq \log a_{SiO_2} < 0$. At comparable P–T, the reaction brucite + silica = chrysotile in serpentinite (e.g. Berman *et al.*, 1986) yields log $a_{SiO_2} < -2$, which makes the matrix a suitable sink for silica while brucite existed. The early subsaturated state of a_{SiO_2} during jadeite formation changed to saturation during albitization. No reaction within the joint serpentinite–jadeitite assemblage at the appropriate conditions can drive such a process. Therefore, the change in a_{SiO_2} must have originated from the metasomatic fluid itself. Increase in a_{SiO_2} occurs in fluid flow down a pressure gradient either at near constant, or possibly slightly up a temperature gradient (Ferry & Dipple, 1991). Silica removed by fluids at depth (or higher P/T conditions) could be the source for higher level assemblages.

Calcium metasomatism is commonly associated with serpentinites and serpentinization. The breakdown of calcic pyroxene during serpentinization of ultramafic rocks yields Ca-bearing fluids (e.g. Barnes & O'Neil, 1969; Coleman, 1980). Metasomatic products of such fluids are rodingites and tremolite-rich reaction rinds around inclusions (Coleman, 1967, 1980). Calcic metasomatism is minor in the field area. The increase in omphacite and (clino)zoisite in jadeitites indicates an increase in calcium metasomatism towards the end of the jadeitization process. Tremolite in the rinds around jadeitite blocks is another example. The rind assemblage is closest to that of the albitites and suggests contemporaneous formation or equilibration.

Barium (and to a lesser extent Sr) enters minerals in these rocks and is apparently related to the serpentinite environment. Banalsite in jadeitite is found in Burma (Harlow & Olds, 1987) and occurs with stronalsite in Japan (Kobayashi *et al.*, 1987). In the albite–mica rocks Ba metasomatism stabilizes celsian, cymrite and barian phengite; Sr is enriched in zoisite. Barium-rich minerals are found in the benitoite occurrence in the New Idria serpentinite body and the cymrite occurrence at Pacheco Pass (Essene, 1967), both in San Benito County, California. Commonly, Ba (and Sr) becomes enriched in silicates through metasomatic/metamorphic reactions that break down sedimentary sulphates (e.g. Bol *et al.*, 1989; Pan & Fleet, 1991). Tectonized serpentinite melanges can destabilize and dissolve barite and celestine through reduction of f_{O_2}, at least during serpentinization (Frost, 1985; and below), and keep Ba and Sr dissolved in fluid in serpentinites (Tatsumi *et al.*, 1986). Such fluids, encountering the Al-rich blocks, will react to form Ba-aluminosilicates.

The presence of graphite in albitites and jadeitites can constrain fluid composition and f_{O_2}. Fluid inclusions in jadeite from a few samples are two-phase aqueous inclusions with about twice seawater salinity and no evidence of CO_2. In the C–O–H system at 400° C (Holloway, 1984), a predominantly aqueous fluid coexisting with graphite will have an f_{O_2} essentially identical to QFM. At 250 °C, a single aqueous fluid coexisting with graphite is constrained to within $-0.2/+3.2 \log_{10}$ units f_{O_2} of QFM. These conditions are consistent with the observed Fe-bearing silicates, e.g. pyroxene and amphibole, that are dominated by neither Fe^{2+} nor Fe^{3+}. The presence of graphite does not represent highly reducing conditions for jadeitites and albitites, in contrast to the serpentinization assemblage Srp + Ol + Brc + Mag where f_{O_2} is 4–5 log units below QFM (Frost, 1985). This difference in f_{O_2} suggests that the strongly reducing conditions of serpentinization ended before jadeitization and albitization occurred.

Tectonic considerations

The serpentinite belts of central Guatemala with their jadeitites and eclogites (McBirney *et al.*, 1967) are evidence for a collision along the southern edge of the Maya Block. The relatively high P/T estimates for jadeitite formation support this conclusion. The jadeitite-bearing zone north of the Motagua River extends only *c.* 15 km, a small section of the serpentinite along the Motagua Fault. The limited extent and rarity of jadeitites suggest unusual and restricted petrogenetic conditions. The interpretation of an oblique collision (Burke, 1988) may have provided the necessary conditions: an early collisional regime underthrust serpentinite to relatively high P–T conditions followed by later back-arc lateral faulting. Low confining pressures in the lateral faults allow flow of a trapped fluid from the subduction wedge to flush the fracturing serpentinite and permit low-a_{SiO_2} soda metasomatism of included tectonic blocks in a moderately high-P/T environment. Serpentinite will ascend diapirically as fault slivers and permit terrane preservation. The rarity of jadeitites world-wide suggests that an unusual but reproducible combination of tectonic events must attend jadeitite formation. Jadeitite petrogenesis may therefore bear significantly on understanding the full range of processes that operate in collisional environments.

ACKNOWLEDGEMENTS

I thank O. Salazar, I. del Cid, and the Instituto Geografico Militar de Guatemala for assistance in Guatemala; E. P. Olds for participation early in the project; T. W. Donnelly and G. Dengo for assistance and discussions about Guatemalan geology; M. L. Ridinger (Jade S.A.), G. Leech (La Case del Jade), the Department of Mineral Sciences of the National Museum of Natural History (Smithsonian Institution) and the Mineralogy Department of the Natural History Museum of Los Angeles County for samples; G. Cavallo for assistance with X-ray diffraction analysis; A. K. El-Shazly for collaboration with the thermodynamic calculations on analcime; and L. Garza-Valdes for samples, discussion and camaraderie. The typescript was greatly improved by reviews of M. Cloos, A. K. El-Shazly, E. Essene, J. Liou and S. Sorensen. This research has been supported by the American Museum of Natural History. Equipment support was provided through NSF grant EAR-89-16687.

APPENDIX

Thermodynamic parameters for analcime

Entropy and enthalpy for analcime were estimated by first calculating potential ranges using the methods of Holland (1989) and Chermak & Rimstidt (1989, 1990), which then were refined through a linear programming approach (see El-Shazly & Liou, 1991) utilizing the experimental data of Manghnani (1970), Liou (1971), Kim & Burely (1971) and Gasparik (1985). Heat capacity values are from Johnson *et al.* (1982). Thermal expansion was estimated by modelling analcime as intermediate with cristobalite and nepheline using values from Clark (1966) and compressibility with values from Clark (1966). Thus, applying Berman's formula:

$$V_{P,T}/V_{1\,\text{bar},298\,\text{K}} = 1 + V_1(T-298) + V_2(T-298)^2 + V_3(P-1) + V_4(P-1)^2;$$

$$V_1 = 3.8\times10^{-5}\,\text{deg}^{-1},\quad V_2 = 0,$$

$$V_3 = -2.5\times10^{-6}\,\text{bar}^{-1} \text{ and } V_4 = 100\times10^{-12}\,\text{bar}^{-2};$$

$$V_0 = 97.49\,\text{cm}^3/\text{mol}.$$

ΔG (kJ/mol)	ΔH (kJ/mol)	S (J/mol·K)	Reference
−3091.73	−3309.839	234.43	Robie *et al.* (1978)
−3077.2	−3296.9	226.75	Johnson *et al.* (1982)
−3091.73	−3310.951	230.20	This study

REFERENCES

Anderson, T. H. & Schmidt, V. A., 1983. The evolution of Middle America and the Gulf of Mexico–Caribbean Sea region during Mesozoic time. *Bulletin Geological Society of America*, **94**, 941–966.
Barnes, I. & O'Neill, J. R., 1969. The relationship between fluids in some fresh Alpine-type ultramafics and possible modern serpentinization, western United States. *Bulletin Geological Society of America*, **80**, 1947–1960.
Berman, R. G., 1988. Internally-consistent thermodynamic data for minerals in the system K_2O–Na_2O–CaO–MgO–FeO–Fe_2O_3–Al_2O_3–SiO_2–TiO_2–H_2O–CO_2–O. *Journal of Petrology*, **29**, 445–522.
Berman, R. G., Brown, T. H. & Perkins, E. H. (1987). *GE0-CALC Software for the Calculation and Display of Pressure–Temperature–Composition Phase Diagrams*. University of British Columbia, Vancouver.
Berman, R. G., Engi, M., Greenwood, H. J. & Brown, T. H., 1986. Derivation of internally-consistent thermodynamic data

by the technique of mathematical programming: a review with application to $MgO–SiO_2–H_2O$. *Journal of Petrology*, **27**, 1331–1364.

Bertrand, J. & Vuagnat, M., 1975. Sur la présence des basaltes en coussins dans la zone ophiolitique méridionale de la cordillere central de Guatémala. *Bulletin suisse de Minéralogie et Pétrologie*, **55**, 136–142.

Bertrand, J. & Vuagnat, M., 1976. Etude pétrographique de diverses ultrabasites ophiolitiques du Guatémala et de leurs inclusions. *Bulletin suisse de Minéralogie et Pétrologie*, **56**, 527–540.

Bertrand, J. & Vuagnat, M., 1977. Données chimiques diverses sur des ophiolites du Guatémala. *Bulletin suisse de Minéralogie et Pétrologie*, **57**, 466–483.

Bertrand, J. & Vuagnat, M., 1980. Inclusions in the serpentinite melange of the Motagua Fault Zone, Guatemala. *Archives des Sciences* (Société de Physique et D'Histoire Naturelle de Genève), **33**, 321–336.

Bol, L. C. G. M., Bos, A., Sauter, P. C. C. & Jansen, J. B. H., 1989. Barium–titanium-rich phlogopites in marbles from Rogaland, southwest Norway. *American Mineralogist*, **74**, 439–447.

Bosc, E. A., 1971. Geology of the San Agustín Acasaguastlan quadrangle and northeastern part of El Progreso quadrangle. *Unpubl. Dissertation, Rice University.*

Burke, K., 1988. Tectonic evolution of the Caribbean. *Annual Review of Earth and Planetary Sciences*, **16**, 201–230.

Carpenter, M. A., 1979. Omphacites from Greece, Turkey, and Guatemala: composition limits of cation ordering. *American Mineralogist*, **64**, 102–108.

Carpenter, M. A., 1981. Omphacite microstructures as time–temperature indicators of blueschist- and eclogite-facies metamorphism. *Contributions to Mineralogy and Petrology*, **78**, 441–451.

Carpenter, M. A. & Smith, D. C., 1981. Solid solution and cation ordering limits in high-temperature sodic pyroxenes from the Nybö eclogite pod, Norway. *Mineralogical Magazine*, **44**, 37–44.

Chermak, J. A. & Rimstidt, J. D., 1989. Estimating the thermodynamic properties (dG_f^0 and dH_f^0) of silicate minerals at 298 K from the sum of polyhedral contributions. *American Mineralogist*, **74**, 1023–1031.

Chermak, J. A. & Rimstidt, J. D., 1990. Estimating the free energy of formation of silicate minerals at high temperatures from the sum of polyhedral contributions. *American Mineralogist*, **75**, 1376–1380.

Chhibber, H. L., 1934. *The Mineral Resources of Burma.* Macmillan, London.

Chihara, K., 1971. Mineralogy and paragenesis of jadeites from the Omi-Kotaki area, Central Japan. *Mineralogical Society of Japan, Special Paper*, **1**, 147–156.

Clark, S. P., Jr., 1966. *Handbook of Physical Constants.* Geological Society of America, New York.

Coleman, R. G., 1961. Jadeite deposits of the Clear Creek area, New Idria district, San Benito County, California. *Journal of Petrology*, **2**, 209–247.

Coleman, R. G., 1967. Low temperature reaction zones and Alpine ultramafic rocks of California, Oregon and Washington. *Bulletin of the U.S. Geological Survey*, **1247**, 1–49.

Coleman, R. G., 1980. Tectonic inclusions in serpentinite. *Archives des Sciences* (Société de Physique et d'Histoire Naturelle de Genève), **33**, 89–102.

Coleman, R. G. & Donato, M. M., 1979. Oceanic plagiogranite revisited. In: *Trondhjemites, Dacites and Related Rocks* (ed. Barker, F.), pp. 149–167. Elsevier Publ. Co., Amsterdam.

Coombs, D. S. & Whetten, J. T., 1967. Composition of analcime from sedimentary and burial metamorphic rocks. *Geological Society of America Bulletin*, **78**, 269–282.

Dipple, G. M. & Ferry, J. M., 1990. Metasomatism in ductile faults caused by fluid flow along temperature gradients. *Abstracts with Programs, Geological Society of America 1990 Annual Meeting*, A213.

Dobretsov, N. L., 1963. Mineralogy, petrography and genesis of ultrabasic rocks, jadeitites, and albitites from the Borus Mountain Range (the West Sayan). Academia Scientifica SSR (Siberian Branch). *Proceedings of the Institute of Geology and Geophysics*, **15**, 242–316.

Dobretsov, N. L., 1984. Problem of the jadeite rocks, associating with ophiolites. *Mineralia slov.*, **16**, 3–12.

Dobretsov, N. L. & Ponomareva, L. G., 1965. Comparative characteristics of jadeite and associated rocks from Polar Ural and Near-Balkhash Region. *Academia Scientifica USSR (Siberian Branch), Trudy, Institute of Geology and Geophysics*, **31**, 178–243. (translation: *International Geology Review*, **10**, 221–279.)

Donnelly, T. W., Horne, G. S., Finch, R. C. & López-Ramos, E., 1990. Northern Central America; The Maya and Chortis Blocks. In *The Geology of North America, Vol. H. The Caribbean Region* (eds Case, J. E. & Dengo, G.), pp. 37–76. Geological Society of America, Boulder.

Duncan, A. P., 1986. The petrologic and tectonic significance of Guatemalan jadeitites. *Unpubl. honor's project, Geology Department, Macalester College, St Paul, MN.*

Edgar, A., 1983. Chemistry, occurrence and paragenesis of feldspathoids: a review. In *Feldspars and Feldspathoids: Structures, Properties and Occurrences* (ed. Brown, W. L.), pp. 501–526. NATO ASI series, Series C. D. Reidel Publishing Co., Dordrecht.

El-Shazly, A. K. & Liou, J. G., 1991. Glaucophane chloritoid-bearing assemblages from NE Oman: petrologic significance and a petrogenetic grid for high P metapelites. *Contributions to Mineralogy and Petrology*, **107**, 180–201.

Ernst, G., 1963. Significance of phengitic micas from low grade schists. *American Mineralogist*, **48**, 1357–1373.

Essene, E. J., 1967. An occurrence of cymrite in the Franciscan Formation, California. *American Mineralogist*, **52**, 1885–1890.

Farver, J. R., 1989. Oxygen self-diffusion in diopside with application to cooling rate determinations. *Earth and Planetary Science Letters*, **92**, 386–396.

Ferry, J. M. & Dipple, G. M., 1991. Fluid flow, mineral reactions, and metasomatism. *Geology*, **19**, 211–214.

Foshag, W. F. & Leslie, R., 1955. Jadeite from Manzanal, Guatemala. *American Antiquity*, **21**, 81–83.

Frost, B. R., 1985. On the stability of sulfides, oxides and native metals in serpentinite. *Journal of Petrology*, **26**, 31–63.

Gasparik, T., 1985. Experimentally determined compositions of diopside–jadeite pyroxene with albite and quartz at 1200–1350° C and 15–34 kbar. *Geochimica et Cosmochimica Acta*, **49**, 865–870.

Goddard, G. & Smith, D. C., 1984. Deux micas inhabituels dans les eclogites de la compointrie (Loire Atlantique): Na–Mg margarite, preiswerkite. *10e Reunion Annuelle des Sciences de la Terre, Bordeaux, 1984 (abstract)*. Soc. Géol. Fr.

Graham, C. M., Tareen, J. A. K., McMillan, P. F. & Lowe, B. M., 1992. An experimental and thermodynamic study of cymrite and celsian stability in the system $BaO–Al_2O_3–SiO_2–H_2O$. *European Journal of Mineralogy*, **4**, 251–269.

Guidotti, C. V., 1984. Micas in metamorphic rocks. In: *Micas, Reviews in Mineralogy* Volume 13 (ed. Bailey, S. W.), pp. 357–456. Mineralogical Society of America, Washington, DC.

Hammond, N., Aspinall, A., Feather, S., Hazelden, J., Gazard, T. & Agrell, S., 1979. Maya jade: source location and analysis. In: *Exchange Systems in Prehistory* (eds Earle, D. K. & Ericson, J. E.), pp. 35–67. Academic Press, New York.

Harlow, G. E., 1986. Jadeitites and their fluid inclusions from Rio Motagua, Guatemala. *IMA 86 Abstracts with Program, International Mineralogical Association 14th General Meeting, Stanford University*, p. 119 (abstract).

Harlow, G. E., 1993. Middle American jade: geologic and petrologic perspectives on its variability and source. In: *Precolumbian Jade, a Proceedings Volume from a Conference on Middle American Jade* (ed. Lange, F. W.), pp. 9–29. University of Utah Press, Salt Lake City.

Harlow, G. E. & Olds, E. P., 1987. Observations on terrestrial ureyite and ureyitic pyroxene. *American Mineralogist*, **72,** 126–136.

Heinrich, W. & Althaus, E., 1980. Die obere Stabilitatsgrenze von Lawsonit plus Albit Bzw. Jadeit. *Fortschritte der Mineralogie*, **58,** 49–50.

Helgeson, H. C., Delany, J. M., Nesbitt, H. W. & Bird, D. K., 1978. Summary and critique of the thermodynamic properties of rock-forming minerals. *American Journal of Science*, **278A,** 1–229.

Hey, M. H., 1954. A new review of the chlorites. *Mineralogical Magazine*, **30,** 277–289.

Holland, T. J. B., 1989. Dependence of entropy on volume for silicate and oxide minerals: a review and a predictive model. *American Mineralogist*, **74,** 5–13.

Holloway, J. R., 1984. Graphite–CH_4–H_2O–CO_2 equilibria at low-grade metamorphic conditions. *Geology*, **12,** 455–458.

Iwao, S., 1953. Albitite and associated jadeite rock from Kotaki District, Japan: a study in ceramic raw material. *Report of the Geological Survey of Japan*, **153.**

Johnson, G. K., Flotow, H. E., O'Hare, P. A. & Wise, W. S., 1982. Thermodynamic studies of zeolites: analcime and dehydrated analcime. *American Mineralogist*, **67,** 736–748.

Keusen, H. R. & Peters, T. J., 1980. Preiswerkite, an Al-rich trioctahedral sodium mica from the Geisspfad ultramafic complex (Penninic Alps). *American Mineralogist*, **65,** 1134–1137.

Kim, K.-T. & Burley, B. J., 1971. Phase equilibria in the system $NaAlSi_3O_6$–$NaAlSiO_4$–H_2O with special emphasis on the stability of analcite. *Canadian Journal of Earth Sciences*, **8,** 311–337.

Kobayashi, S., Miyake, H. & Shoji, T., 1987. A jadeite rock from Oosa-cho, Okayma Prefecture, Southwestern Japan. *Mineralogical Journal*, **13,** 31–327.

Kretz, R., 1983. Symbols for rock-forming minerals. *American Mineralogist*, **68,** 277–279.

Lacroix, M. A., 1930. La jadéite de Birmanie; les roches qu'elle constitue ou qui l'accompagnent. Composition et origine. *Bulletin de la Société français de Minéralogie*, **53,** 216–254.

Lasnier, B. & Smith, D. C., 1989. A ferro-alumino taramite- and glaucophane-bearing eclogite from the French Armorican Massif: Ile Dumet. *Terra Cognita*, **9,** 17 (abstract).

Liou, J. G., 1971. Analcime equilibria. *Lithos*, **4,** 389–402.

Liou, J. G., Maruyama, S. & Cho, M., 1985. Phase equilibria and mineral parageneses of metabasites in low-grade metamorphism. *Mineralogical Magazine*, **49,** 321–42.

Manghnani, M. H., 1970. Analcime–jadeite phase boundary. *Physics of Earth and Planetary Interiors*, **3,** 456–516.

Massonne, H. J. & Schreyer, W., 1987. Phengite geobarometry based on the limiting assemblage with K-feldspar, phlogopite and quartz. *Contributions to Mineralogy and Petrology*, **96,** 212–224.

McBirney, A. R., 1963. Geology of a part of the Central Guatemalan cordillera. *University of California Publications in Geological Sciences*, **38,** 177–242.

McBirney, A. R., Aoki, K.-I. & Bass, M., 1967. Eclogites and jadeite from the Motagua fault zone, Guatemala. *American Mineralogist*, **52,** 908–918.

Meyer, J., 1983. The development of the high-pressure metamorphism in the Allalin metagabbro (Switzerland). High pressure metamorphism: indicator of subduction and crustal thickening. *Terra Cognita*, **3,** 187.

Morimoto, N., Fabries, J., Ferguson, A. K., Ginzburg, I. V., Ross, M., Seifert, F. A., Zussman, J., Aoki, K. & Gottardi, G., 1988. Nomenclature of pyroxenes. *American Mineralogist*, **73,** 1123–1133.

Morkovkina, V. F., 1960. Jadeitites in the hyperbasites of the Polar Urals. *Izvestia Akademia Nauk SSSR, series geologia*, **4.**

Newcomb, W., 1975. Geology, structure, and metamorphism of the Chuacús group, Río Hondo Quadrangle and vicinity, Guatemala. *Unpubl. Dissertation, State University of New York at Binghamton.*

Pan, Y. & Fleet, M. E., 1991. Barian feldspar and barian–chromian muscovite from the Hemlo area, Ontario. *Canadian Mineralogist*, **29,** 481–498.

Perfit, M. R. & Heezen, B. C., 1978. The geology and evolution of the Cayman Trench. *Geological Society of America Bulletin*, **89,** 1155–1174.

Philippott, P. & Selverstone, J., 1991. Trace-element-rich brines in eclogitic veins: implications for fluid composition and transport during subduction. *Contributions to Mineralogy and Petrology*, **106,** 417–430.

Pindell, J. L. & Dewey, J. F., 1982. Permo-Triassic reconstruction of western Pangea and the evolution of the Gulf of Mexico/Caribbean region. *Tectonics*, **1,** 179–212.

Robie, R. A., Hemingway, B. S. & Fisher, J. R., 1978. Thermodynamic properties of minerals and related substances at 298.15 K and 1 bar (10^5 Pascals) pressure and at higher temperatures. *U.S. Geological Survey Bulletin*, **1452.**

Schwartz, D. P., Cluff, L. S. & Donnelly, T. W., 1979. Quaternary faulting along the Caribbean–North American plate boundary in Central America. *Tectonophysics*, **52,** 431–445.

Selverstone, J., Moretani, G. & Staude, J. M., 1991. Fluid channelling during ductile shearing: transformation of granodiorite into aluminous schist in the Tauern Window, Eastern Alps. *Journal of Metamorphic Geology*, **9,** 419–431.

Silva, Z. C. G., 1970. Origin of albitites from eastern Guatemala. *Boletim dos Servicos de Geologia e Minas* (Brazil), **22,** 23–32.

Smith, D. C., 1988. A review of the peculiar mineralogy of the "Norwegian coesite–eclogite province", with crystal–chemical, petrological, geochemical and geodynamic notes and an extensive bibliography. In: *Eclogites and Eclogite-Facies Rocks* (ed. Smith, D. C.), pp. 1–206. Elsevier, Amsterdam.

Tatsumi, Y., Hamilton, D. L. & Nesbitt, R. W., 1986. Chemical characteristics of fluid phase released from a subducted lithosphere and origin of arc magmas: evidence from high-pressure experiments and natural rocks. *Journal of Volcanology and Geothermal Research*, **29,** 293–309.

Takayama, M., 1986. Mode of occurrence and significance of jadeite in the Kamuikotan metamorphic rocks, Hokkaido, Japan. *Journal of Metamorphic Geology*, **4,** 445–454.

Thompson, A. B., 1971. Analcite–albite equilibria at low temperatures. *American Journal of Science*, **271,** 79–92.

Thompson, J. B. & Thompson, A. B., 1976. A model system for mineral facies in pelitic schists. *Contributions to Mineralogy and Petrology*, **58,** 243–277.

Tilley, C. E., 1956. Nepheline associations. *Koninklijk Nederlandsch Geologisch Mijnbouwkundig Genootschap*, **16,** 1–11.

Tlili, A., Smith, D. C., Beny, J. M. & Boyer, H., 1989. A Raman microprobe study of natural micas. *Mineralogical Magazine*, **53,** 165–179.

Wadge, G. & Burke, K., 1983. Neogene Caribbean plate rotation and associated Central American tectonic evolution. *Tectonics*, **2,** 633–643.

Woodland, A. B. & Walther, J. V., 1987. Experimental determination of the solubility of the assemblage paragonite, albite, and quartz in supercritical H_2O. *Geochimica et Cosmochimica Acta*, **51,** 365–372.

Yoder, H. S., Jr, 1950. The jadeite problem; pts. I and II. *American Journal of Science*, **248,** 225–248, 312–334.

Yund, R. A. & Tullis, J., 1983. Subsolidus phase relations in the alkali feldspars with emphasis on coherent phases. In: *Feldspar Mineralogy* (ed. Ribbe, P. H.), pp. 141–176. Mineralogical Society of America.

Received 27 April 1992; revision accepted 20 April 1993.